Polar Biology
https://doi.org/10.1007/s00300-018-2338-x

REVIEW

Influence of summer conditions on surface water properties and phytoplankton productivity in embayments of the South Shetland Islands

Claudia Aracena[1] · Humberto E. González[2,3] · José Garcés-Vargas[2,3] · Carina B. Lange[3,4,5] · Silvio Pantoja[4,5] · Francisca Muñoz[6] · Elisabeth Teca[2] · Eduardo Tejos[7]

Received: 15 September 2017 / Revised: 30 April 2018 / Accepted: 7 May 2018

Abstract

Phytoplankton productivity in glaciomarine embayments of the West Antarctic Peninsula is constrained because of extensive thermohaline variability, which is due to seasonal sea-ice and glacial melting. To determine whether or not this affects the biology of the water column, we explored the influence of surface water properties on phytoplankton productivity in four embayments of the South Shetland Islands (SSI) during late summer of 2013. We analyzed hydrographic, climatic, and primary productivity satellite data (wind velocity, sea-ice cover, and chlorophyll-a), in situ CTD measurements of physical and chemical characteristics, new estimates of net primary production (NPP), and surface water samples for chlorophyll-a, nutrients, biogenic silica, and plankton composition. Sea-ice cover at the SSI was ~ 20% during February. Long-term satellite wind data (2010–2015) showed that during February 2013 the average wind velocity was ~ 2 m s^{-1} higher than the long-term mean with two low sea surface temperature events occurring simultaneously at all sites. The CTD profiles did not show vertical salinity changes, although salinity was highly correlated with the percentage of integrated nanoplankton Chl-*a*, which represented > 50% of the total integrated Chl-*a* in all the embayments. Phytoplankton was the major contributor to the integrated carbon biomass of the upper water column, where centric diatoms predominated. The contribution of microzooplankton and bacterioplankton at the different sites explained NPP values and the trophic mode at each site. Specifically, NPP at Fildes Bay exhibited an autotrophic productivity mode in contrast to Collins Bay, where both heterotrophic and autotrophic modes alternated, mainly due to weekly changes in community respiration rates.

Keywords South Shetland Islands · Antarctica · Chlorophyll-*a* · Net primary production · Biogenic silica · Nutrients · Phytoplankton

Introduction

The decrease of glacier ice mass, the reduction of the sea-ice season (Cook et al. 2005; Martinson et al. 2008; Stammerjohn et al. 2008), and the increase of precipitation along

Electronic supplementary material The online version of this article (https://doi.org/10.1007/s00300-018-2338-x) contains supplementary material, which is available to authorized users.

✉ Claudia Aracena
claudia.aracena@umag.cl

[1] Centro de Investigación GAIA Antártica, Universidad de Magallanes, Avenida Bulnes 01855, Casilla 113 D, Punta Arenas, Chile

[2] Instituto de Ciencias Marinas y Limnológicas, Universidad Austral de Chile, Campus Isla Teja, Edificio Emilio Pugín, Valdivia, Chile

[3] Centro FONDAP de Investigación en Dinámica de Ecosistemas Marinos de Altas Latitudes (IDEAL), Universidad Austral de Chile, Campus Isla Teja, Edificio Emilio Pugín, Valdivia, Chile

[4] Centro COPAS Sur-Austral, Universidad de Concepción, Casilla 160-C, Concepción, Chile

[5] Departamento de Oceanografía, Universidad de Concepción, Casilla 160-C, Concepción, Chile

[6] Plancton Andino SpA, Terraplén # 869, Puerto Varas, Chile

[7] Laboratorio de Estudios Ambientales, Departamento de Química Ambiental, Universidad Católica de la Santísima Concepción, Casilla 297, Concepción, Chile

the West Antarctic Peninsula (WAP) (Thomas et al. 2008) have impacts on the thermohaline structure of the water column, the circulation of water masses and stratification, constraining the ability of primary producers to incorporate carbon from the atmosphere. In terms of salinity, the Southern Ocean (SO) is the most affected, exceeding the trends observed in other oceans (Rhein et al. 2013). In fact, it has been reported that, within the glaciomarine environments of the WAP, biomass and composition of phytoplankton have decreased (Garibotti et al. 2005; Ducklow et al. 2007; Montes-Hugo et al. 2009; Schloss et al. 2012). On the other hand, at Palmer Station, sea-ice associated with increased seasonal concentration of chlorophyll-*a* (Chl-*a*) and characterized by a high proportion of diatoms likely favorable for the Antarctic krill has increased since 2009 (Schofield et al. 2017).

The glaciomarine embayments of the South Shetland Islands (SSI) in the WAP constitute a key natural laboratory to study the effects of local climate and seasonal melting on aquatic productivity. These coastal ecosystems are extremely sensitive to climate variations due to the presence of vast glaciers, whose fluctuations could affect the hydrography and biological production because of increased seasonal freshwater flux into the surface ocean. In fact, the WAP has been identified as the fastest warming region of the Southern Hemisphere and the region of greatest warming in the world, with increases of both atmospheric and oceanic temperatures of 5 and 1 °C, respectively, over the past 50 years (Meredith and King 2005; Abram et al. 2013). In this region, the increase in heat is associated with warm, saline Upper Circumpolar Deep Water (UCDW) that penetrates onto the WAP shelf (Schofield et al. 2017). This heat supply by UCDW is associated with stronger winds over the SO (Thompson and Solomon 2002; Marshall 2003), which, accompanied by increased summertime surface-ocean heating (Meredith and King 2005), has caused strong retreats in the seasonal sea-ice cover (Stammerjohn et al. 2008) and an 87% reduction of glaciers in the area (Cook et al. 2005).

Montes-Hugo et al. (2009) estimated a ~ 12% decrease in phytoplankton blooms due to increased glacial melt on phytoplankton communities in the WAP during 1998–2006. Their study demonstrated that the magnitude of phytoplankton blooms has changed latitudinally, especially at the northern WAP, and is associated with more cloudy days, greater upper mixed layer depth, stronger intensity winds, and shorter sea-ice seasons along the marginal ice zone. The decline of sea-ice in the Antarctic ecosystem and associated physical space–time changes in its structure and functioning are believed to be the determining factor in reductions throughout the pelagic food web (Schofield et al. 2010; Saba et al. 2014). By contrast, the opposite trend of increasing phytoplankton biomass over time reflects increased duration and area of ice-free water during the summer season in the southern areas of the WAP (Montes-Hugo et al. 2009). Similarly, the 20-year time series collected by the Palmer Long-Term Ecological Research program (United States Palmer Research Station) to assess long-term patterns and stability in the coastal phytoplankton communities in the WAP (Schofield et al. 2017) showed a significant increase in the seasonally integrated concentration of Chl-*a*, with diatoms being the dominant phytoplankton group. In general, the continental shelves and marginal ice zones around Antarctica display a much higher phytoplankton biomass and productivity than open ocean regions (Arrigo et al. 1998). Phytoplankton composition (Villafañe et al. 1995; Kang et al. 2002; Schloss et al. 2014) in combination with Chl-*a* and primary production estimates (Holm-Hansen and Mitchell 1991; Varela et al. 2002; Holm-Hansen and Hewes 2004) have shown that summer phytoplankton is dominated by microphytoplankton > 20 µm in different ecological regions of the Drake Passage, Bransfield Strait, and the WAP, with a strong spatial salinity gradient between the different water bodies (Hewes et al. 2009). Chl-*a* biomass at the South Shetland Islands (SSI) rarely shows concentrations higher than 3 mg m^{-3} (Hewes et al. 2009), although the largest phytoplankton bloom recorded over the last 20 years had a maximum of 20 mg m^{-3} in coastal waters of southern King George Island in January 2010 (Schloss et al. 2014).

Recently, oceanographic research has focused on examining the possible impact of climate change on the phytoplankton inhabiting the waters of the SO south of the Subtropical Front (Deppeler and Davidson (2017). During the past two decades, the consequences of rapid recent warming and freshening on marine productivity of several areas close to the SSI have been investigated. Phytoplankton blooms were monitored long term (Schloss et al. 2014) to observe their seasonal variability (Hewes et al. 2009), community composition (Schofield et al. 2017) and physiological responses due to changes in light, vertical mixing (Schloss and Ferreyra 2002; Schloss et al. 2002) and salinity effects (Hernando et al. 2015). The influences of local weather on physical and chemical changes in the water column and on the phyto- and zooplankton communities of coastal glaciomarine environments of the SSI remain unresolved.

In this study, we explored the influences of surface water properties on primary productivity proxies (BSi, Chl-*a*, carbon biomass, and phytoplankton abundances) during late summer in four glaciomarine embayments of the SSI, an area with abrupt changes due to extended glacial and sea-ice melt. Our analysis focused on ice coverage, wind field data, as well as in situ measurements of water physical–chemical properties from 1 to 50 m depth (sea surface temperature, dissolved oxygen, salinity, fluorescence, pH, and turbidity), and chemical–biological characteristics from 1 to 25 m depth (nutrients, BSi concentration, Chl-*a* concentration, net primary production (NPP), carbon biomass, and phytoplankton,

microzooplankton, and bacterioplankton abundances and composition). Our late summer results supplement previous information available on phytoplankton and environmental conditions in the SSI (Kopczynska 2008; Hewes et al. 2009; García Muñoz et al. 2013; Schloss et al. 2002, 2012, 2014; Hernando et al. 2015) and improve our understanding of the environmental factors that control plankton abundance and composition along the WAP. Although limited in time (summer) and space (SSI), our results contribute recent information to facilitate detecting reference sites for mesoscale changes and trends in SSI plankton communities, and to compare with other international monitoring programmes. Additionally, our findings on BSi concentration as a proxy of autotrophic diatom production may enable calibrating paleo-data, such as paleoproductivity changes in polar and sub-polar regions.

The SSI is an island arc off the northern coast of the AP, comprising Robert, Nelson, Greenwich, Livingston, Deception, and King George islands, that have sufficient proximity to glacial ice to permit detection of a glacial signature within the sediments (Powell and Domack 2002). The outlet and valley glaciers in the area terminate as tidewater glaciers (Simms et al. 2011) that ablate mainly by calving icebergs during the summer months when sea surface temperatures are above freezing (Khim et al. 2007). This results in a vertical sediment flux controlled by summer melting processes that cause sediment-laden meltwater plumes to form (Hass et al. 2010) and prevent phytoplankton growth (Schloss et al. 2012).

King George Island is the largest island of the South Shetland archipelago and reaches a maximum altitude ~ 700 m above sea level with a maximum ice cap thickness of 395–422 m (Simoes et al. 2004; Blindow et al. 2010). About 90% of its surface (1250 km^2) is glaciated by several connected ice caps with pronounced outlet glaciers (Rückamp et al. 2011; Rückamp and Blindow 2012). Despite the extensive cover of ice caps and snowfields, some low-lying peninsulas are ice-free during summer. A distinct glaciomarine environment occurs on Deception Island (Fig. ESM_4, in online resource), an active volcano which is part of the SSI and located in southwest Bransfield Strait. Natural fertilization processes that occur in and around Deception Island and meltwater are sources of potentially bioavailable iron (Monien et al. 2011) which offers a key environment to elucidate the mechanics of primary production in a changing ocean (Hewes et al. 2009) (see texts 1 and 2 in online resource as electronic supplementary material).

Our study sites were located in Bransfield Strait, which is a transition zone between the Bellingshausen and Weddell Seas. The Bransfield Strait waters result from coastal and oceanic circulation processes that combine through freshwater flow, heat transport, and atmospheric circulation. A thermohaline front, described as the Peninsula Front (PF) (Sangrà et al. 2017), lies between the colder and saltier Transitional Weddell Waters (TWW) in the southeastern section of the Bransfield Strait, whereas fresher and warmer waters are associated with the Transitional Bellingshausen Waters in the northwestern section (Gonçalves-Araujo et al. 2015). The flow along the northern flank of the SSI is associated with the Southern Antarctic Circumpolar Current Front (Orsi et al. 1995), a dominant component of the large-scale circulation of the SO (Mura et al. 1995; García Muñoz et al. 2013; Sangrà et al. 2014). In situ data and laboratory experiments in the Bransfield Strait by Sangrà et al. (2017) suggest that our study sites could be influenced by the position of the PF and the anticyclonic circulation of eddies in the Strait, which are constrained by the circulation dynamics of the Bransfield Current (Niiler et al. 1991) which flows northeastward along the SSI coasts.

Materials and methods

In order to observe the influence of late summer climatic conditions on water column properties, we selected four sampling stations in the SSI and one in Isabel Riquelme Island (IRI) on the south side of the Bransfield Strait close to the mainland WAP. Surface water column characteristics were determined from in situ sampling and measurements of physical, chemical, and biological characteristics at each station (Fig. 1). Late summer climatic conditions were resolved from long- and short-term satellite data on sea-ice percentage, wind speed, direction, and sea surface temperature (SST). To determine if the satellite wind data represented local conditions at Fildes Bay, we correlated satellite with local data on wind velocity available between 16 and 22 February 2016 at the Eduardo Frei station (62.1931°S, 58.9825°W) from Dirección Meteorológica de Chile (http://164.77.222.61/RedEmaNacional/php/VisorMMA.php?codigoNacional=950001) with the nearest pixel of the wind-derived product ASCAT METOP-A (62.125°S, 58.875°W) (Fig. ESM_1, online resource).

Satellite data

We used February satellite data (encompassing latitudes 61.5°–64.0°S and longitudes 63.0°–57.0°W) on sea-ice coverage (period 2013–2015) extracted from a grid rectangle (2° in latitude × 4° in longitude) centered in the glaciomarine embayments of the SSI, except for Deception Island where no pixel with data was found. We also obtained long-term satellite data on wind strength and direction from 2010 to 2015 and Chl-*a* concentrations from 2003 to 2015. Additionally, February anomalies were computed for Chl-*a* concentration. We extracted satellite daily SST for February 2013 from a grid rectangle (5° in latitude × 8°

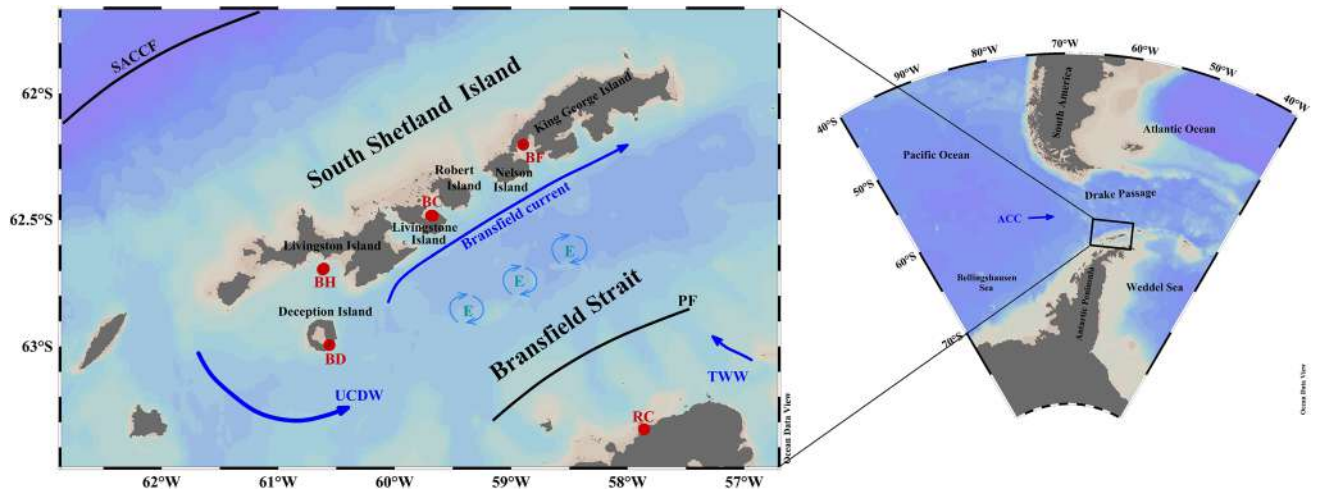

Fig. 1 Study area in the South Shetland Islands (enlargement) off the Antarctic Peninsula. *Red dots* denote sampling stations during the summer of 2013. *BF* Fildes Bay, *BC* Chile Bay, *BH* Hanna Bay, *BD* Deception Bay, *RC* Rada Covadonga. The circulation of the Bransfield Strait described by Sangrà et al. (2017) includes the occurrence of anticlockwise eddies (*E*) along the central basin that are constrained by the Bransfield Current (*blue arrow*, *BC*), and the Peninsula Front (*PF*). *ACC* Antarctic Circumpolar Current, *SACCF* Southern Antarctic Circumpolar Current Front, *UCDW* Upper Circumpolar Deep Water, *TWW* Transitional Weddell Water. (Color figure online)

in longitude) centered in the glaciomarine embayments of the SSI (Fig. 1, red dots). Daily SST time series were obtained for each embayment averaging the grid rectangle (Fig. EMS_2, online resource). Datasets were downloaded from https://coastwatch.pfeg.noaa.gov/erddap/index.html ERDDAP. Sea-ice coverage was obtained from https://seaice.uni-bremen.de/sea-ice-concentration/information (Sea-Ice Remote Sensing at the University of Bremen).

Surface wind magnitude and direction were obtained from a product developed by L'Institut Français de Recherche pour l'Exploitation de la Mer. The product was interpolated by the objective method and based on the product derived by the Advanced Scatterometer (ASCAT METOP-A) with a spatial resolution of 0.25° × 0.25° (Bentamy and Fillon 2012).

Sea-ice coverage was obtained from the satellite Shizuku (GCOM-W1) which carries the new sensor Advanced Microwave Scanning Radiometer-EOS (the successor of AMSR-E) (Spreen et al. 2008). This sensor provides daily data with a spatial resolution of approximately 6 × 4 km. Satellite-derived images of Chl-*a* concentrations were obtained from the Moderate Resolution Imaging Spectroradiometer (MODIS) sensor onboard the Aqua satellite (Savtchenko et al. 2004). The Ocean Biology Processing Group of NASA provides a monthly product of surface-ocean Chl-*a* concentration with a spatial resolution of ~ 4 km.

The Multi-scale Ultra-high Resolution SST product is derived from 8 satellites objectively interpolated through the MUR (Multi-sensor Ultra-high Resolution) analysis, with a spatial resolution of 0.011° × 0.011° (Chin et al. 2013). MUR uses the MRVA (Multi-Resolution Variation Analysis) technique, which is based on wavelet decomposition.

Physical, chemical, and biological characteristics in the water column

Surface water column conditions were determined from in situ measurements of physical, chemical, and biological characteristics at each sample station. The sampling period was during late summer (20 February–1 March) of 2013 during the oceanographic campaign ECA 49 onboard the vessel AP41 "Aquiles." The stations were Fildes Bay (BF), Chile Bay (BC), Hanna Bay (BH), Deception Bay (BD), and Rada Covadonga (RC), which is the only station located outside the SSI range (Fig. 1, red dots). At each station, a CTD Seabird 19 plus with auxiliary sensors for dissolved oxygen (membrane sensor SBE 43), turbidity and fluorescence (optic sensor ECO FLNTU), and pH was deployed to 50 m water depth, with the exception of station BC, where the cast recorded 27 m water depth due to the proximity to the bottom (Table ESM_1, in online resource). The data were processed with the SBED data software to obtain downcast values averaged over 1-m depth intervals (Table 1).

Water samples were collected by Go-Flow 10-L bottles at 6 depths in the water column (1, 2.5, 5, 10, 15, and 25 m) to determine vertical variations in nutrient (nitrate, orthophosphate, and silicic acid) and biogenic silica concentrations (BSi). The samples were filtered at the scientific base "Profesor Julio Escudero" from the Antarctic Chilean Institute (INACh) and analyzed at the Organic Geochemistry and Paleoceanography laboratories of the

Department of Oceanography at the University of Concepción. We also measured total and fractionated Chl-*a* (> 20 µm, 20–2 µm, < 2 µm), phytoplankton, microzooplankton, and bacterioplankton abundances at the Biological Oceanography Laboratory at the Institute of Marine and Limnological Sciences of the Universidad Austral de Chile.

Dissolved macronutrient concentrations were determined according to the method of Strickland and Parsons (1972). Two replicates were analyzed with a UV–VIS spectrophotometer following the colorimetric methods of Strickland and Parsons (1972). BSi concentration was obtained in two replicates following the method of Ragueneau et al. (2005) (Table 2). Particulate organic carbon (POC) and particulate organic nitrogen (PON) were estimated from a 0.5-L sample filtered through pre-combusted MFS filters and stored frozen (− 20 °C) until analysis, following standard procedures (Bodungen et al. 1991). In the laboratory, measurements were determined with a Europa-Hydra 20–20 continuous flow isotope ratio mass spectrometer after combustion at 1000 °C at the UC Davis Stable Isotope Facility Laboratory.

Total and fractionated Chl-*a* contents were obtained using the method described by Parsons et al. (1984), which consists of a 24-h extraction with 10 mL of a 90% acetone solution. After extraction, the Chl-*a* concentration of each sample was measured in a TD-700 Turner fluorometer (Table 2). The values of total and fractionated Chl-*a* were integrated between six depths in the water column (Table 3).

We used a 50-mL water sample from each station and depth preserved with 2% glutaraldehyde to count the heterotrophic and autotrophic organisms (Tables 2, 3). This allowed the quantification of bacterioplankton using epifluorescence microscopy (Porter and Feig 1980), which relies on the use of specific 4′, 6-diamidino-2-2-phenylindole (DAPI) fluorochrome that binds to bacterial DNA. Samples were observed with a fluorescence microscope and UV light ~ with 365-nm excitation. Bacterioplankton as total heterotrophic bacteria abundances were transformed to biomass in µg C L^{-1} by assuming 8.3 fg C per cell (Fuhrman and Azam 1982), as previously used to quantify bacterioplankton at the SSI (Llanos et al. 1991).

Finally, quantification and taxonomical description of phytoplankton and microzooplankton were performed with an inverted microscope (Nikon Eclipse TS100) following the method of Utermöhl (1958) and using the taxonomical works of Cupp (1943), Beers and Stewart (1970), Reynolds (1997), Tomas (1997), and Boltovskoy (1999). Because our fieldwork was time-limited, we estimated microzooplankton abundances using the same sample as for phytoplankton. This method can underestimate microzooplankton, but it is useful for learning more about their specific groups, because it avoids losing individuals and inducing changes in their morphology by manipulation and preservation, especially of ciliates and flagellates (Sherr and Sherr 1994).

We calculated the carbon biomass of phytoplankton and microzooplankton from cell biovolume based on geometric assignation (Edler 1979).

In situ primary production estimations

During late summer 2013, in situ gross primary production (GPP) and community respiration (CR) were estimated using the methodology described by Winkler (1888) and modified by Strickland and Parsons (1972). Due to adverse weather conditions at sites in Chile Bay, Deception Bay, and Rada Covadonga, we measured GPP and CR only in Fildes and Hanna bays. For comparative purposes, we also included results on GPP and CR obtained during March 2015 at Fildes, Collins, and Maxwell bays (Table 4). The collected water was incubated in 125-mL borosilicate bottles at 1, 5, 10, and 25 m depths. Three bottles were immediately fixed to have the initial concentration of dissolved oxygen, whereas the other three clear and dark bottles were incubated in situ for 8 h. After the incubation period, in situ GPP was estimated using oxygen production/consumption in the clear and dark bottles, respectively. In situ GPP estimations were depth-integrated (mg C m^{-2} h^{-1}) using a trapezoidal integration of the euphotic zone (1–25 m). Results on both GPP and CR were expressed in mg C m^{-2} day^{-1}, considering ~ 15 h

Table 1 Location of sampling stations and CTD values for physical–chemical parameters averaged over 1–25 m depth during summer of 2013 in four glaciomarine embayments of the Southern Shetland Islands, and one site at Isabel Riquelme Island

Station	Sampling data	Latitude (S)	Longitude (W)	Temperature (C)	Salinity	Fluorescence (mg m^{-3})	Turbidity (NTU)	Oxygen (ml L^{-1})	pH
BF	1 March 2013	62.2	58.92	1.3	34.1	3.1	0.1	7.6	8.2
BC	20 February 2013	62.48	59.7	1.1	34.1	1.9	0.5	7.2	8.2
BH	21 February 2013	62.69	60.61	1.2	34.1	1.7	0.1	7.2	8.1
BD	22 February 2013	62.99	60.56	1.8	33.9	8	0.5	8.1	8
RC	23 February 2013	63.33	57.91	− 1.1	34.4	0.4	0	7.3	8.1

The values are averaged. Stations are *BF* Fildes Bay, King George Island; *BC* Chile Bay, Greenwich Island *BH* Hanna Bay, Livingston Island; *BD* Deception Bay, Deception Island; *RC* Rada Covadonga, Isabel Riquelme Island

Table 2 Chemical and biological characteristics of the upper water column (1–25 m depth) at four stations in the South Shetland Islands

Sampling sites	Depth (m)	Nitrate (μM)	Standard deviation	Orthophosphate (μM)	Standard deviation	Silicic acid (μM)	Standard deviation	Biogenic silica (mM)	Standard deviation	Total Chl-*a* (mg m^{-3})
Station BF	1	13.06	0.01	1.36	0.00	27.97	3.36	0.39	0.01	3.26
Fildes Bay	2.5	21.11	0.00	1.45	0.02	66.36	3.35	0.39	0.01	2.87
King George Island (KGI)	5	14.27	0.01	1.12	0.05	25.70	1.14	0.38	0.00	4.17
	10	8.83	0.01	1.26	0.10	18.77	1.37	0.37	0.00	2.93
	15	24.28	0.02	1.44	0.02	63.92	4.50	0.37	0.00	3.07
	25	11.04	0.00	1.21	0.04	20.65	5.32	0.36	0.00	2.63
Station BC	1	7.42	0.03	4.36	0.19	38.35	9.07	0.16	0.00	1.02
Chile Bay	2.5	21.29	0.00	1.56	0.02	27.67	4.77	0.20	0.00	1.23
Greenwich Island (GI)	5	9.72	0.02	1.29	0.05	18.90	3.50	0.21	0.00	1.35
	10	17.71	0.06	1.65	0.06	26.50	6.34	0.20	0.01	1.04
	15	19.91	0.04	1.37	0.01	52.89	0.02	0.23	0.00	1.14
	25	12.95	0.02	1.22	0.04	16.43	4.75	0.23	0.00	1.22
Station BH	1	22.48	0.02	1.44	0.02	54.61	0.05	0.20	0.02	1.28
Hanna Bay	2.5	19.65	0.03	1.36	0.01	59.58	5.52	0.20	0.00	1.55
Livingstone Island (LI)	5	11.71	0.03	1.64	0.01	31.70	7.65	0.18	0.01	1.35
	10	22.93	0.02	1.76	0.01	63.46	0.04	0.14	0.00	1.02
	15	14.54	0.01	1.61	0.05	30.81	2.96	0.20	0.00	0.84
	25	20.91	0.00	1.97	0.03	25.86	2.30	0.18	0.00	1.12
Station BD	1	5.34	0.01	0.78	0.01	31.06	2.15	0.51	0.01	3.71
Deception Bay	2.5	11.99	0.02	0.63	0.01	84.52	0.09	0.44	0.00	5.48
Deception Island (DI)	5	16.69	0.01	0.66	0.02	81.26	0.15	0.36	0.01	3.27
	10	9.09	0.02	0.60	0.02	27.19	0.95	0.39	0.00	6.54
	15	9.85	0.01	1.03	0.05	29.76	0.82	2.90	0.00	7.06
	25	10.02	0.00	0.98	0.04	18.55	4.33	1.04	0.00	3.58
Station RC	1	14.52	0.22	1.85	0.02	31.06	6.42	0.24	0.03	0.16
Rada Covadonga	2.5	17.48	0.00	2.34	0.01	32.05	1.22	0.20	0.00	0.34
Isabel Riquelme Island (IRI)	5	25.51	0.00	1.82	0.00	–	–	0.13	0.00	0.41
	10	11.34	0.01	1.58	0.04	19.46	1.43	0.22	0.02	0.44
	15	25.02	0.00	1.86	0.01	70.99	0.05	0.16	0.00	0.21
	25	15.91	0.04	3.30	0.00	26.92	0.85	0.14	0.00	0.36

Table 2 (continued)

Sampling sites	Depth (m)	Chl-*a* > 20 µm (mg m^{-3})	Chl-*a* 20–2 µm (mg m^{-3})	Chl-*a* < 2 µm (mg m^{-3})	Centric diatoms (µg C L^{-1})	Pennate diatoms(µg C L^{-1})	Total Phytoplankton (µg C L^{-1})	Dinoflagellates (µg C L^{-1})	Ciliates (µg C L^{-1})	Total microzooplankton (µg C L^{-1})	Total bacteria (µg C L^{-1})	Total biomass (µg C L^{-1})
Station BF	1	1.25	1.88	0.13	13.05	0.16	13.20	0.59	1.15	1.74	2.58	17.52
Fildes Bay	2.5	0.64	2.07	0.17	16.13	5.89	22.02	0.78	0.20	0.98	2.23	25.23
King George Island (KGI)	5	1.77	2.07	0.33	12.26	0.18	12.45	0.50	0.20	0.70	2.10	15.24
	10	0.64	2.16	0.12	2.55	0.04	2.59	0.08	0.08	0.16	1.53	4.28
	15	1.09	1.89	0.09	3.64	0.02	3.66	0.06	0.08	0.14	–	3.80
	25	0.24	2.21	0.18	2.66	0.06	2.71	0.10	0.24	0.34	1.54	4.60
Station BC	1	0.05	0.91	0.06	0.78	0.14	0.92	0.04	0.07	0.11	1.82	2.85
Chile Bay	2.5	0.34	0.86	0.03	1.16	0.23	1.39	0.06	0.07	0.13	1.65	3.18
Greenwich Island (GI)	5	0.47	0.81	0.07	1.36	0.28	1.64	0.07	0.57	0.64	1.32	3.60
	10	0.02	0.96	0.06	0.73	0.17	0.89	0.04	0.29	0.32	1.45	2.67
	15	0.00	1.06	0.08	0.85	0.18	1.03	0.04	0.50	0.54	1.52	3.09
	25	0.32	0.83	0.07	0.35	0.00	0.35	0.02	0.14	0.17	1.73	2.24
Station BH	1	0.50	0.70	0.08	0.20	0.32	0.51	0.05	0.11	0.16	1.21	1.89
Hanna Bay	2.5	0.76	0.68	0.12	0.62	0.55	1.16	0.10	0.00	0.10	1.35	2.61
Livingstone Island (LI)	5	0.60	0.67	0.08	0.62	0.38	1.00	0.13	0.11	0.25	1.20	2.45
	10	0.34	0.55	0.13	0.52	0.07	0.59	0.15	0.00	0.15	1.67	2.41
	15	0.30	0.47	0.07	0.77	0.05	0.82	0.09	0.40	0.49	1.29	2.59
	25	0.51	0.52	0.09	0.23	0.02	0.25	0.05	0.07	0.12	1.46	1.83
Station BD	1	0.30	2.54	0.87	8.49	0.26	8.75	0.00	0.00	0.00	8.45	17.20
Deception Bay Island (DI)	2.5	1.64	3.47	0.37	11.82	0.04	11.86	0.00	0.00	0.00	4.40	16.26
	5	1.13	1.91	0.23	21.44	0.07	21.51	0.11	0.99	1.11	5.53	28.14
	10	2.78	3.53	0.24	25.71	0.05	25.77	0.24	1.59	1.83	5.55	33.15
	15	0.00	7.06	0.00	22.36	0.07	22.43	0.18	1.19	1.37	5.50	29.30
	25	0.00	3.48	0.09	13.18	0.06	13.24	0.16	0.00	0.16	4.35	17.75
Station RC	1	0.06	0.06	0.03	0.87	0.02	0.90	0.05	0.00	0.05	0.49	1.43
Rada Covadonga	2.5	0.17	0.15	0.03	0.63	0.02	0.65	0.01	0.08	0.09	0.38	1.12
Isabel Riquelme Island (IRI)	5	0.22	0.12	0.06	0.67	0.02	0.68	0.08	0.07	0.15	0.70	1.54
	10	0.26	0.11	0.07	0.40	0.01	0.41	0.09	0.00	0.09	0.43	0.93
	15	0.08	0.10	0.03	0.54	0.02	0.56	0.04	0.00	0.04	0.53	1.13
	25	0.13	0.12	0.11	0.44	0.02	0.46	0.03	0.00	0.03	0.63	1.13

The variables include nutrient concentrations (nitrate, orthophosphate, and silicic acid), proxies of autotrophic biomass (total and fractionated Chl-*a*, biogenic silica, and carbon biomass), and plankton biomass (phytoplankton, microzooplankton, and bacterioplankton)

Table 3 Values of productivity variables in the surface water column integrated from 1 to 25 m depths at the five stations in the South Shetland Islands

Station	Chl-*a*-Total (mg m$-^2$)	Chl_*a* > 20 µm (mg m$-^2$)	Chl-*a*-20-2 µm (mg m$-^2$)	Chl-*a* < 2 µm (mg m$-^2$)	Microplankton %	Nanoplankton %	Picoplankton %	Total phytoplankton (mg C m$-^2$)	Centric diatoms (mg C m$-^2$)
BF	74.6	21.5	49.3	3.8	28.8	66.1	5.1	154.6	141.4
BC	28.1	3.9	22.3	1.9	13.9	79.4	6.6	23.6	19.7
BH	26.1	10.6	13.3	2.2	40.6	50.9	8.5	16.8	13.2
BD	117.4	8.0	104.0	5.4	6.8	88.6	4.6	474.2	472.6
RC	7.9	3.8	2.7	1.4	48.0	34.1	17.9	13.1	12.7

Station	Pennate diatoms (mg C m^{-2})	Dinoflagellates (mg C m$-^2$)	Ciliates (mg C m^{-2})	Total microzooplankton (mg C m^{-2})	Total bacterioplankton (mg C m^{-2})	Total biomass (mg C m^{-2})	Total phytoplankton %	Total bacterioplankton %	Total microzooplankton %
BF	13.2	5.2	4.2	9.4	41.1	205.1	75.4	20.0	4.59
BC	3.8	1.0	8.2	9.2	36.9	69.7	33.8	52.9	13.26
BH	3.5	2.4	3.8	6.2	33.4	56.4	29.8	59.2	11.05
BD	1.6	3.71.0	20.6	24.4	126.6	625.2	75.8	20.3	3.90
RC	0.4	1.3	0.4	1.7	13.0	27.8	47.0	46.8	6.20

BF Fildes Bay, *BC* Chile Bay, *BH* Hanna Bay, *BD* Deception Bay, *RC* Rada Covadonga. Total and fractionated chlorophyll-*a* (Chl-*a*); total biomass of the main groups of phytoplankton and microzooplankton, and bacterioplankton

for a photosynthetic day (Fig. EMS_3, in online resource) and 24 h for respiration, respectively. Finally, net primary production (NPP) was calculated as the difference between GPP and CR (NPP = GPP − CR).

Results

Satellite data

The seasonal sea-ice coverage (monthly mean 2013–2015) showed a similar trend in almost all embayments, with low percentages in a range of ~ 5% to 25% between November and June, and > 40% between July and October. The only exception was the station located at Rada Covadonga (RC), in Isabel Riquelme Island, where the percentage of sea-ice was substantially higher between June and October (40–75%), while during the rest of the year it was similar to the other embayments (Fig. 2a). These data also showed a different pattern in the timing of the high sea-ice season between the SSI and IRI. In the latter, sea-ice covered > 40% of the Rada Covadonga area from June until October, reaching a maximum of ~ 70% between July and August. In the SSI, high sea-ice cover percentage only persisted between August and September with a maximum of 60% (Fig. 2b).

In general, the long-term (2010–2015) mean surface wind velocity ranged between 4 and 8 m s^{-1} (Fig. 3a). Moreover, during late summer 2013, mean wind velocity increased to ~ 6 and 8 m s^{-1} (Fig. 3b). The daily average in situ wind speed obtained from the Eduardo Frei meteorological station (62.1931°S, 58.9825°W) correlated very well with the daily satellite data ($R^2 = 0.947$; $p = 0.002$) (Fig. ESM_1, online resource). Therefore, we can confidently extrapolate the satellite results to the SSI stations.

Satellite monthly long-term SST (2003–2015) was highest during February near our study sites (Fig. EMS_2, online resource). The SST pattern in February 2013 was similar in all SSI embayments, with fluctuations between 0 and 2 °C; however, station RC at IRI fluctuated between − 1.5 and 0°C (Fig. 3c). Two events of low SSTs were observed during 4–6 and 17–19 February at all stations, with the latter being the most extreme, lowering SST by ~ 1 °C. Thereafter, SST remained constant at all stations (Fig. 3c). Daily satellite SST results were highly correlated with averaged in situ SST (1–25 m depth) for each station ($R^2 = 0.970$; $p = 0.002$). Therefore, satellite SST data can be validated with our in situ SST measurements at the five stations.

The Chl-*a* concentrations (mg m^{-3}) derived from satellite information ranged from 0.3 to 2 mg m^{-3} for the long-term February mean (2003–2015). Those data revealed an isolated longitudinal patch with Chl-*a* concentration > 2 mg m^{-3} located at the northern margin of the SSI extending between 58.5°W and 61.5°W (Fig. 4a). In contrast, the mean Chl-*a* concentrations for February 2013 were lower (range: 0.1– > 1 mg m^{-3}) with a less extensive spatial distribution than the 12-year long-term mean (Fig. 4b). Indeed, a negative anomaly < − 1 mg m^{-3} was observed along the northern and southern flanks of the South Shetlands Islands arc (Fig. 4c).

Table 4 Gross primary production (GPP), community respiration (*CR*) estimations, and plankton composition in Hanna Bay and Fildes Bay during summer 2013, and Collins Bay, Maxwell Bay, and Fildes Bay during summer 2015

Station	Date	Integrated depth interval (m)	GPP (mg C m^{-2} h^{-1})	CR (mg C m^{-2} h^{-1})	GPP (mg C m^{-2} h^{-1})	CR (mg C m^{-2} h^{-1})	NPP (mg C m^{-2} h^{-1})
Hanna Bay	21 February 2013	1–5	9.1	10.7			
		5–10	30.6	14.4			
		10–25	57.9	40.0	1.5	1.6	-0.1
Fildes Bay	27 February 2013	1–5	40.8	5.1			
		5–10	46.5	5.6			
		10–25	44.8	7.6	2.0	0.4	1.6
Fildes Bay	1 March 2013	1–5	39.6	1.3			
		5–10	48.5	1.6			
		10–25	63.6	0.0	2.3	0.1	2.2
Collins Bay	27 February 2015	1–5	4.0	5.5			
		5–10	5.1	13.3			
		10–25	0.0	64.6	0.1	2.0	-1.9
Maxwell Bay	3 March 2015	1–5	9.9	15.2			
		5–10	57.0	64.2			
		10–25	195.3	157.2	3.9	5.7	-1.7
Fildes Bay	4 March 2015	1–5	9.2	1.3			
		5–10	45.7	1.7			
		10–25	140.8	28.3	2.9	0.8	2.2
Collins Bay	7 March 2015	1–5	40.0	2.4			
		5–10	48.4	2.6			
		10–25	107.5	7.9	2.9	0.3	2.6

Station	Date	Integrated depth interval (m)	Total phytoplankton (mg C m^{-2})	Total microzooplankton (mg C m^{-2})	Total bacterioplankton (mg C m^{-2})	Dominant plankton group	Trophic mode	Proximity to glaciers
Hanna Bay	21 February 2013	1–5						
		5–10						
		10–25	16.8	6.2	33.4	Bacterioplankton	Heterotrophic	Distal
Fildes Bay	27 February 2013	1–5						
		5–10						
		10–25	142.7	31.4	42.1	Phytoplankton	Autotrophic	Distal
Fildes Bay	1 March 2013	1–5						
		5–10						
		10–25	154.6	9.4	41.1	Phytoplankton	Autotrophic	Distal
Collins Bay	27 February 2015	1–5						
		5–10						
		10–25	226.1	323.9	92.5	Dinoflagellates	Heterotrophic	Proximal
Maxwell Bay	3 March 2015	1–5						
		5–10						
		10–25	161.3	591.6	89.6	Dinoflagellates	Heterotrophic	Intermediate
Fildes Bay	4 March 2015	1–5						
		5–10						
		10–25	90.3	79.0	78.6	Phytoplankton	Autotrophic	Distal
Collins Bay	7 March 2015	1–5						
		5–10						
		10–25	100.7	60.3	68.4	Phytoplankton	Autotrophic	Proximal

Total biomass of phytoplankton, microzooplankton, and bacterioplankton. NPP > 1 = Autotrophic community; NPP < 1 = Heterotrophic community. Proximity to glaciers is near to far (proximal to distal)

GPP Gross primary production, *NPP* net primary production (NPP = GPP − CR)

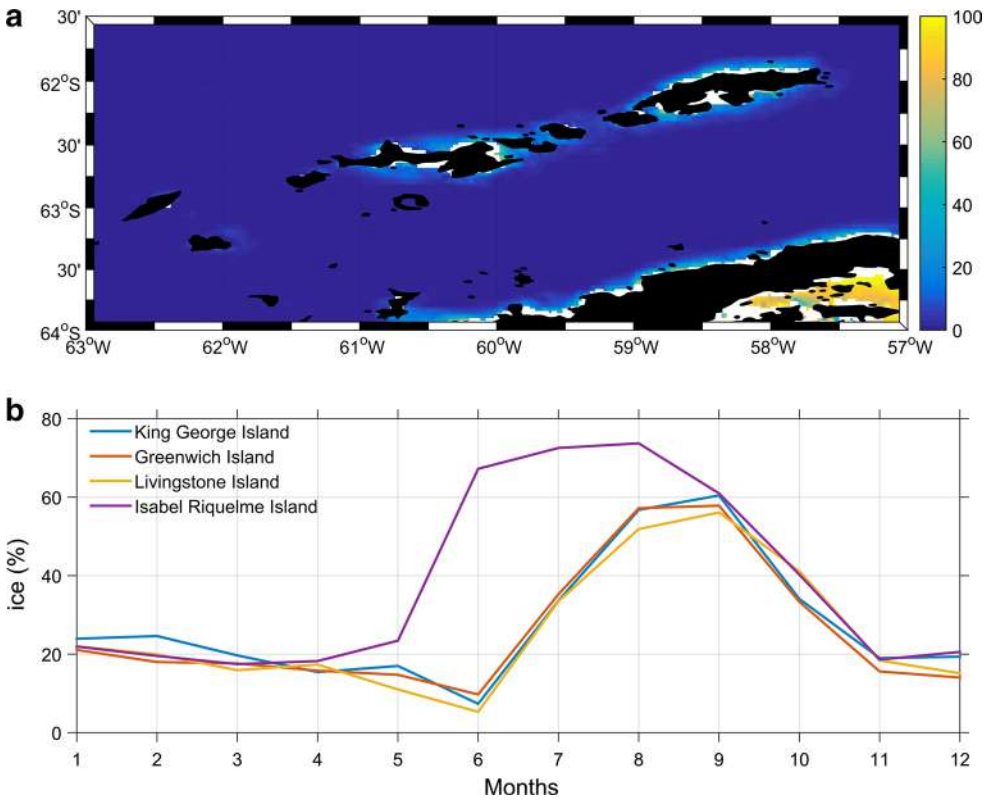

Fig. 2 Sea-ice coverage (%) from AMSR2 (the successor of AMSR-E) obtained from https://seaice.uni-bremen.de/sea-ice-concentration/information. **a** February 2013 mean. *Color scale to the right* indicates percentage. **b** Monthly long-term mean (2013–2015) extracted from a grid rectangle (2° in latitude × 4 ° in longitude) centered in the glaciomarine embayments of the SSI, except Deception Island where no pixel with data was found. (Color figure online)

CTD data

The vertical profiles of temperature and salinity did not vary vertically in the surface water column for stations BF, BH, and RC, or at station BC, where measurements reached 27 m depth. At those stations, SST averaged between − 1.1 and 1.3 °C and surface salinity between 34.1 and 34.4 (Table 1; Fig. 5a). In contrast, temperature and salinity at station BD markedly differed vertically (ranges 2.0–0.8 °C and 32.7–33.9, respectively). At station BD, warm waters (~ 2 °C) of the upper 10 m of the water column decreased gradually to ~ 0.8 °C at 50 m depth (Fig. 5a; Table ESM_1 in online resource). On the other hand, the lowest salinity (~ 32.5) occurred in the upper 2 m of the water column at station BD. Below that depth, salinity increased abruptly to ~ 34 and presented a homogeneous vertical profile down to 50 m depth (Fig. 5a). Temperatures < 0 °C were found only at station RC, with consistent temperature vertically ~ − 1.1 °C (Fig. 5a; Table ESM_1 in online resource).

Average turbidity values were relatively low at all stations (< 0.6 NTU; Table 1; Fig. 5b). At BC, vertical distribution of turbidity peaked (~ 1.3 NTU) between 22 and 24 m depth (Fig. 5b; Table ESM_1). The lowest turbidity values were found at station RC, averaging 0.02 NTU. The vertical fluctuation in turbidity at that station ranged between 0 and 0.08 NTU (Fig. 5b; Table ESM_1).

Averaged fluorescence values ranged from < 0.5 to ~ 8 mg m^{-3} at all stations (Table 1), with variations in the vertical distribution among stations (with the exception of station BC; Fig. 5b, Table ESM_1). Stations BF and BD had the highest fluorescence values (~ 4 and 9 mg m^{-3}, respectively) at depths > 20 m (Fig. 5b). Values < 1 mg m^{-3} were observed only at station RC, where the vertical distribution was homogeneous (Fig. 5b; Table ESM_1).

Averaged pH values were similar at all stations, ranging from 8.04 at BD to 8.24 at BF (Fig. 5c; Table 1). Only station BD presented vertical variability and low pH value (6.9) at the surface (Fig. 5c; Table ESM_1).

Dissolved oxygen concentrations were relatively consistent at stations BF, BC, and RC (ranging from 7.2 to 7.6 ml L^{-1}). At station BH, oxygen concentration was ~ 8 ml L^{-1} at the surface and decreased abruptly to ~ 6.8 ml L^{-1} at ~ 4 m depth. Below 4 m, oxygen concentration increased again to ~ 7.3 ml L^{-1}. The highest averaged oxygen concentration (8.1 ml L^{-1}) was observed at Station BD (Table 1), with a vertical distribution varying from 7.8 to 8.2 ml L^{-1} between 1.8 and 16 m water depth. Below this depth, oxygen decreased to 7.1 ml L^{-1} (Fig. 5c; Table ESM_1).

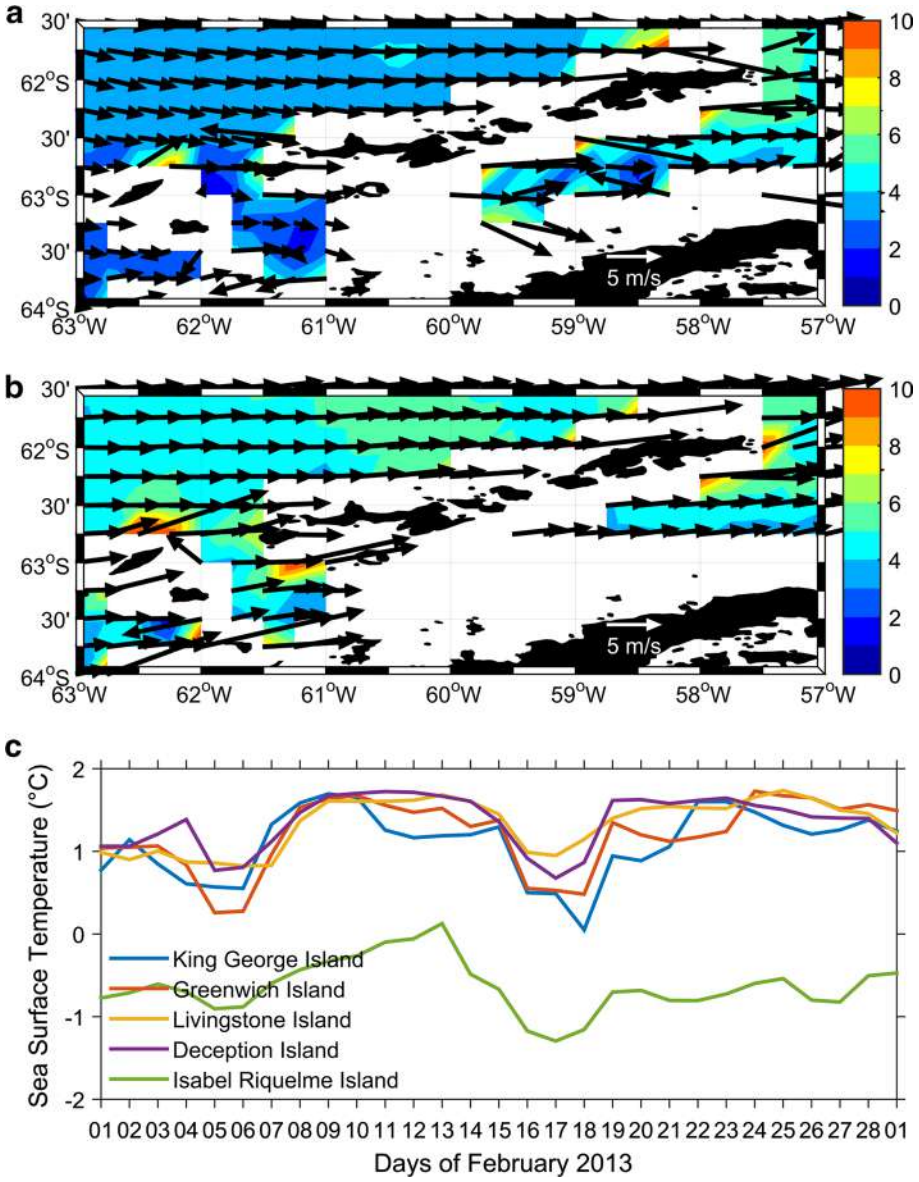

Fig. 3 **a** Long-term February mean (2010–2015), and **b** 2013 February mean of ASCAT wind vector and magnitude in the SSI area (m s^{-1}). *Color bars* in (**a**) and (**b**) relate to wind magnitude from low (*blue*) to high intensity (*red*). *White areas* no data. **c** Daily time series (February 2013) of sea surface temperature (Multi-scale Ultra-high Resolution product) of the SSI embayments. (Color figure online)

Chemical characteristics of the surface water column

Nutrient concentrations in the five embayments of our study (Fig. 6; Table 2) revealed the highest averaged (0–25 m) nitrate concentration at station BH (18.7 µM) and the lowest at station BD (10.5 µM). In general, the vertical distribution of nitrate had two concentration peaks, at 2.5 or 5 m, and at 15 m water depth (> 15 µM; Table 2; Fig. 6a). Exceptions to this pattern occurred at station BH, with peaks > 20 µM at 1 and 10 m depth, and at station BD, which had a homogeneous distribution of ~ 10 µM below 10 m water depth. Average orthophosphate concentration was highest at station RC (2.1 µM) and lowest at station BD (0.8 µM). Station RC also displayed large vertical fluctuations of orthophosphate, ranging from 1.58 to 3.30 µM (Table 2). At other sampling sites, concentrations were relatively homogeneous throughout the upper water column, except at station BC where the high surface concentration (~ 4.4 µM) contrasted with lower values (1.65–1.22 µM) below 2.5 m depth (Table 2). Overall, silicic acid concentrations were high at all stations, with average concentrations of 30.12 µM (BC), 36.09 µM (RC), 37.23 µM (BF), 44.33 µM (BH), and 45.39 µM (BD) (Table 2). Vertical variability of silicic acid was high, although most of the stations had lower values at the surface and subsurface peaks (> 50 µM) at 3–5 m and/or 10–15 m water depth. Remarkably, the highest subsurface values (> 80 µM) were recorded at station BD (Table 2; Fig. 6a).

Biogenic silica (BSi) concentrations were obtained at the same depths as the nutrients. Station BD showed the highest averaged value 0.94 mM and the highest BSi concentration (2.9 mM at 15 m water depth; Table 2; Fig. 6b). At

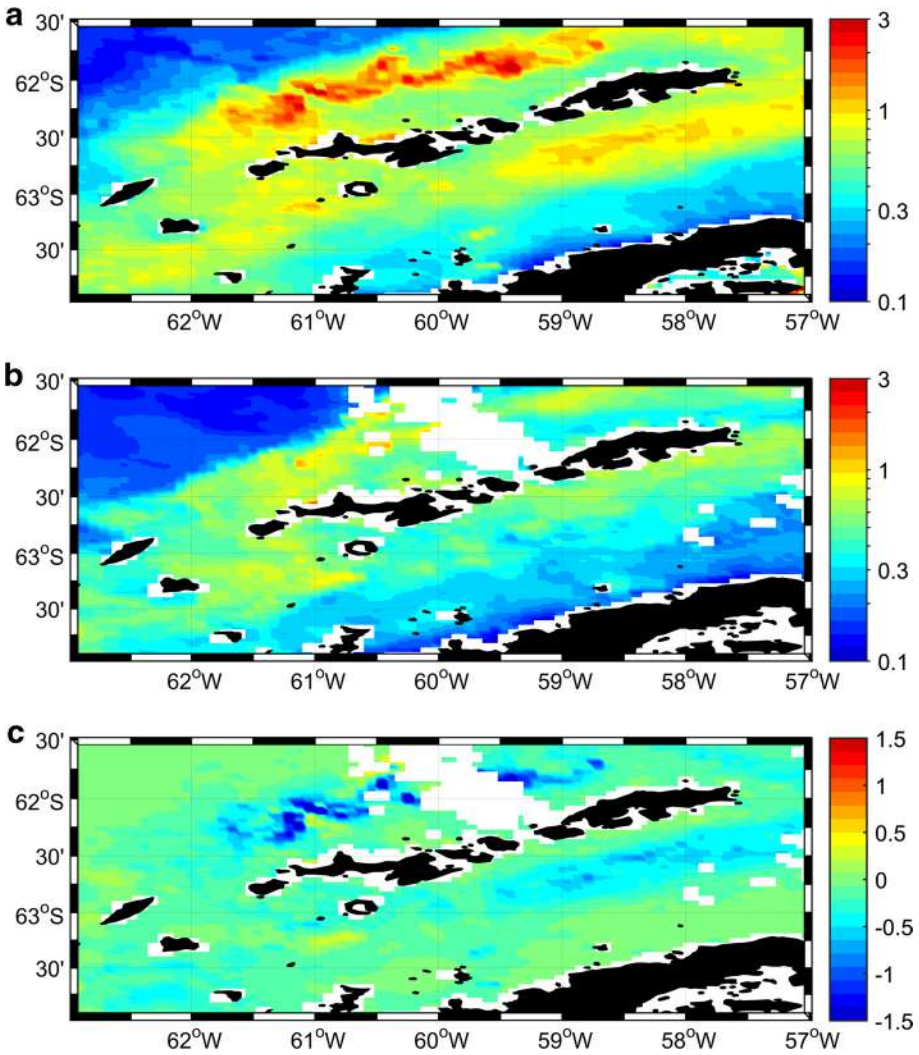

Fig. 4 Aqua MODIS chlorophyll-*a* concentration images (mg m^{-3}). **a** Long-term February mean (2003–2015); **b** 2013 February mean; **c** 2013 February anomalies in relation to the long-term February mean presented in (**a**). *Color bars* in (**a**) and (**b**) relate to chlorophyll-*a* concentrations, and in (**c**) refer to anomalies. (Color figure online)

all other stations, BSi concentrations were relatively low (0.13–0.39 mM) with small fluctuations vertically (Table 2).

Averaged POC contents in the 0–25 m water column ranged from 110.5 µg C L^{-1} (station RC) to 402.5 µg C L^{-1} (station BD). Station BD showed the highest vertical variability, where POC content of ~ 818.5 µg C L^{-1} at 1 m depth abruptly decreased to 334.7 µg C L^{-1} at 5 m depth (Fig. 6b). Below 5 m depth, POC at all stations gradually decreased and values < 100 µg C L^{-1} were found only at station RC (Table 2; Fig. 6b). In general, abrupt vertical gradients of PON occurred in the first 3–5 m depth (Table 2). Averaged PON concentrations ranged between ~ 43.0 µg N L^{-1} (station RC) and ~ 107.6 µg N L^{-1} (station BD) (Table 2).

Chlorophyll-*a*, plankton composition, and primary production

The distributions of total and fractionated Chl-*a* (> 20 µm, 20–2 µm, and < 2 µm) differed vertically at stations BF (range of total Chl-*a* 2.6–4.1 mg m^{-3}) and BD (range of total Chl-*a* 3.7–7.1 mg m^{-3}). Values were homogenous throughout the water column in the other three embayments (Table 2; Fig. 6c). Integrated values of fractionated Chl-*a* showed that the nanoplankton fraction (Chl-*a* 20–2 µm) was the most abundant size class, contributing ≥ 50% of the total Chl-*a*, except at station RC where the microplankton size class (Chl-*a* > 20 µm) prevailed (Table 3).

Phytoplankton was the major contributor to the integrated carbon biomass at stations BF and BD (75.4 and 75.8%, respectively). The highest phytoplankton biomass occurred at station BD (average 17.26 µg C L^{-1}), followed by station BF (average 9.43 µg C L^{-1}). Vertical variability in the water column was high at both locations, with subsurface carbon peaks at 3 m (BF; 22.02 µg C L^{-1}) and 5–15 m depth (BD; 21.51–25.77 µg C L^{-1}) (Table 2; Fig. 6d). In contrast, the other three stations displayed very low phytoplankton biomass (averages: BC = 1.03 µg C L^{-1}; BH = 0.64 µg C L^{-1}; RC = 0.61 µg C L^{-1}), with minor vertical fluctuations (Table 2; Fig. 6d). Radial and multipolar centric diatoms (*Thalassiosira* spp., vegetative cells of *Chaetoceros* spp.,

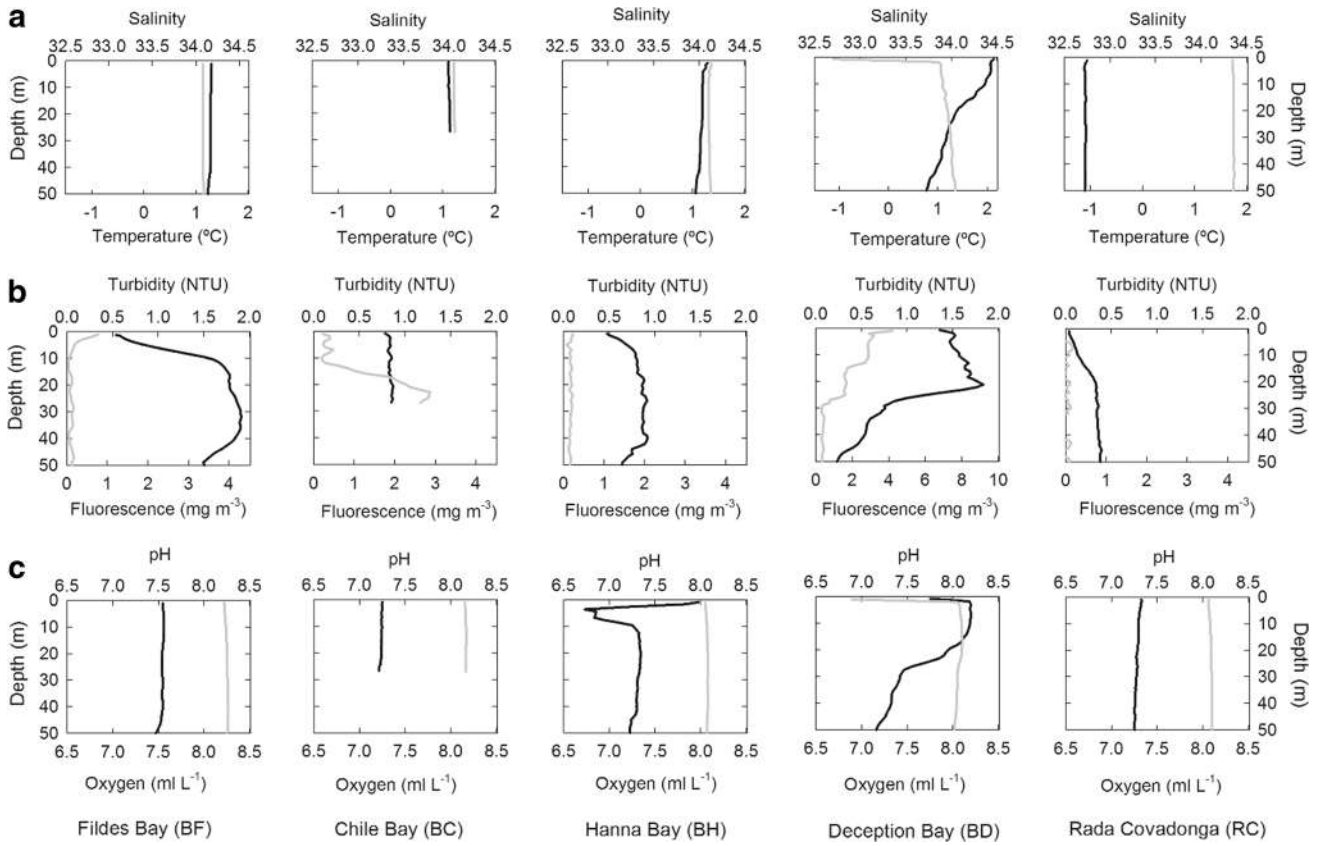

Fig. 5 Vertical distribution of physical and chemical water column properties of the upper 50 m of the water column during summer of 2013 at the five embayments of this study: **a** temperature (*black line*), and salinity (*gray line*); **b** fluorescence (*black line*), and turbidity (*gray line*); **c** oxygen (*black line*), and pH (*gray line*). *BF* Fildes Bay, *BC* Chile Bay, *BH* Hanna Bay, *DB* Deception Bay, *RC* Rada Covadonga.

Corethron pennatum) contributed > 78% of the total integrated phytoplankton carbon. Stations BC and BH were characterized by raphide pennate diatoms (*Pseudo-nitzschia* spp., *Navicula* spp.) and ciliates, both representing > 32% of the total integrated carbon (Table 3).

Bacterioplankton was an important contributor to the integrated carbon biomass during late summer 2013, especially at stations BC and BH (52.9 and 59.2%, respectively). Bacterioplankton was ten times higher (126.6 mg C m^{-2}) at station BD than at the other sites (Table 3), whereas at RC it was the lowest (13.0 mg C m^{-2}).

Microzooplankton at the SSI was a minor contributor to the integrated carbon biomass, ranging between 4.6 and 13.3%. Dinoflagellates dominated the microzooplankton biomass (5.2 mg C m^{-2}) at station BF, but ciliates were more important (20.6 mg C m^{-2}) at station BD (Table 3).

Adverse wind conditions resulting from local short-term events occurred during our sampling dates in February/March 2013 and prevented our measurement of in situ gross primary production (GPP) and community respiration (CR) at all stations. Those incubations were carried out only at stations BF and BH (Table 4). At station BF, GPP estimates were similar on late February and early March sampling dates (1.98 and 2.28 g C m^{-2} day^{-1}, respectively), but CR was lower in March (Table 4). At station BH, both GPP and CR had similar values (1.5 and 1.6 g C m^{-2} day^{-1}, respectively; Table 4). When we had the opportunity to resample Fildes Bay (BF) in March 2015 and measure GPP, we observed higher GPP and CR values (2.93 and 0.752 g C m^{-2} day^{-1}, respectively) than in late summer of 2013. To assess the trophic ecosystem behavior in sites proximal and distal to Collins glacier, we also estimated NPP, as well as plankton abundances and composition at Fildes, Collins, and Maxwell Bays during February 27, and March 7, 2015. In Collins Bay, CR > PP at the end of February, whereas the opposite was found 8 days later (Table 4). Finally, when comparing all stations, Collins Bay stands out with the highest GPP and CR values (Table 4).

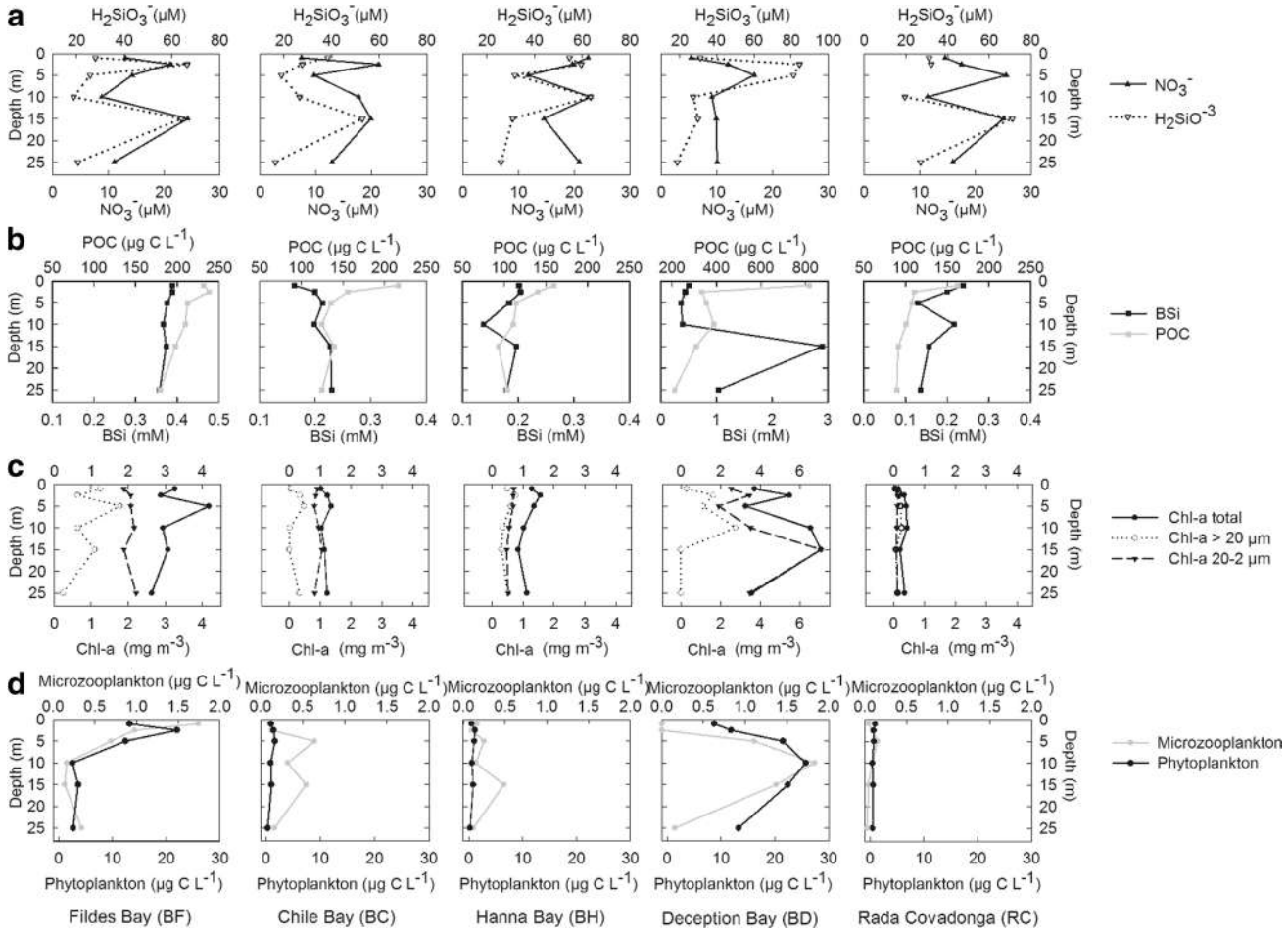

Fig. 6 Vertical distribution of chemical and biological water column properties at the SSI embayments: **a** silicic acid and nitrate concentrations; **b** particulate organic carbon and biogenic silica; **c** total and fractionated chlorophyll-*a*; **d** biomass of microzooplankton and phytoplankton. Data correspond to samples obtained during late summer of 2013 for the five embayments of this study: *BF* Fildes Bay, *BC* Chile Bay, *BH* Hanna Bay, *DB* Deception Bay, *RC* Rada Covadonga

Discussion

Phytoplankton provides key ecosystem services for the SO, because it modulates marine life diversity, global ocean biogeochemistry, and climate due to its role in the photosynthetic absorption of anthropogenic atmospheric carbon excess. However, in the coastal systems of the SO, hydrographic conditions are influenced by seasonal reduction of sea-ice cover, glacier melting, and breakup of the ice shelves, causing freshening and, consequently, constraining phytoplankton abundance and composition. The review by Deppeler and Davidson (2017) suggests that all regions of the SO will experience changes in phytoplankton productivity and composition with climate change, but high variability within and among regions can be expected. Despite variation in phytoplankton abundance and composition between shore and open waters in the WAP, seasonal differences appear to be related to changes in wind velocity and direction, inflow of the Bransfield Strait waters, ice melting, and changes in atmospheric pressure (Kopczynska 2008). However, the net change in sea-ice cover has been strongly suggested to underlie observed changes in the coastal ecosystems of the WAP (Smith et al. 1996; Ducklow et al. 2007). Evidence for that includes a shift in size distribution from large to small phytoplankton cells (Moline et al. 2004; Montes-Hugo et al. 2008), with marked declines in phytoplankton biomass and krill (Saba et al. 2014). In order to understand the present day, and to predict future scenarios of summer ocean productivity in polar/sub-polar regions, our description contributes valuable information on how environmental forcing associated with sea-ice cover, wind velocity, and SST would impact NPP and plankton biomass.

Marine ecosystems located in the SSI region constitute a natural laboratory to investigate the influence of hydrographic and oceanographic changes on primary production. These glaciomarine environments are located in the

transition zone between the Weddell and Bellingshausen seas in an area with intensive ocean circulation processes and influenced by the most extensive ice loss seen during the past two decades (Vaughan et al. 2013). Therefore, research stations in this area should be nominated to be reference sites to continue long-term monitoring, as occurred previously at the Bransfield Strait (Holm-Hansen and Mitchell 1991), in the SSI (Hewes et al. 2009), at PALMER Station (Schofield et al. 2017), Admiralty Bay (Kopczynska 2008), and Potter Cove (Schloss and Ferreyra 2002; Schloss et al. 2002).

We used satellite data on ice cover percentage, wind velocity and direction, SST, and Chl-*a* concentration to compare synoptic regional descriptions with in situ variability on hydrography and plankton productivity in glaciomarine environments from the AP. The satellite data showed the lowest ice coverage of ~ 20% (Fig. 2a, b) and high wind strength mean ~ 6 m s^{-1} (Fig. 3b) during February 2013. During this period, wind was 2 m s^{-1} higher than the long-term February mean of the ASCAT wind vector (Fig. 3a). This seasonal increasing trend was also reported by Montes-Hugo et al. (2009) during mid- to late-summer, when wind speeds were 61% higher in 1998–2006 than in 1978–1986.

In general, SST shows frequent decreases that require 2 or 3 days to stabilize (Fig. 3c). SSTs during our sampling period (20 February–1 March 2013) were relatively stable in comparison with two former events of marked SST decrease (4–6 and 16–18 February) that occurred simultaneously in all embayments (Fig. 3c). Such local variability in SST is associated with the frontal system described in the meteorological charts along the WAP (Carrasco 2007) and likely is influenced by intrusions of cold UCDW towards the Bransfield Strait (Martinson and McKee 2012; Sangrà et al. 2017). The UCDW is derived from the ACC that flows along the continental slope of the WAP (Klinck 1998) (Fig. 1). The presence of the UCDW on the continental shelf has been associated with an increasing trend in the Southern Annular Mode (SAM) that has been linked to an intensification of the westerly winds and a rise in the ocean heat flux (Martinson et al. 2008).

Satellite ocean color sensor data are widely used for detection, mapping, and monitoring of phytoplankton blooms because Earth observation provides a spatially and temporally synoptic view of the ocean (Blondeau-Patissier et al. 2014). On a longer time scale, comparing Hewes et al. (2009) SeaWiFS composite image (average February 1998–2007) with our long-term satellite Chl-*a* results (2003–2015) along the SSI, over the last 12 years the opposite pattern was evident with mean Chl-*a* concentrations ≥ 1 mg m^{-3} even at the northwest margin of the SSI (Fig. 4a). However, during February 2013, satellite-derived Chl-*a* concentration was relatively low < 1 mg m^{-3} (Fig. 4b), possibly due to higher wind velocities that actively mixed the surface water column, prevented stratification, and reduced phytoplankton biomass to nanoplankton size in the SSI embayments. There, satellite Chl-*a* averaged biomass was described as low (1.37 ± 1.0 mg m^{-3}; Hewes et al. 2009), but exceptionally large summer blooms of 20 mg m^{-3} were also reported recently in coastal waters of southern King George Island (Schloss et al. 2014). Our in situ total Chl-*a* values (0.16–7.06 mg m^{-3}) were in the range described previously, despite the fact that our results are relatively lower at stations BC, BH, and RC, and higher at stations BF and BD.

We found local signatures of the SSI, IRI, and BD on the physical, chemical, and biological characteristics of the surface and subsurface water column. These shallow coastal areas are exposed to strong seasonal salinity fluctuations in the productive season, but their local variability in the ice extent and duration throughout the year had not previously been reported. The satellite data at IRI indicated that more than 40% of sea-ice cover lasted 5 months (during June until October), whereas at the SSI sea-ice cover persisted only 2 months (August and September). At PALMER Station, south of our sites, favorable conditions for phytoplankton growth include high winter sea-ice extent and duration (Saba et al. 2014) of at least 3.3 months (Stammerjohn et al. 2012), leading to a shallow winter mixed layer and strong stratification. This condition enhances water column stability in the following spring and summer due to increased sea-ice melt water (Saba et al. 2014). However, we do not extend this interpretation to our sites because our data on ice cover extent show a very site-specific signature for SSI and IRI. Additionally, in shallow embayments, high wind speed produces mixing of the upper water column, resuspension of glacier flow, which reduces stratification, phytoplankton growth, and, subsequently, the higher trophic levels due to spatial and temporal changes in the distribution of phytoplankton biomass and size (Moline et al. 2004; Montes-Hugo et al. 2008; Schloss et al. 2014; Schofield et al. 2017).

The distribution of phytoplankton biomass around or near the SSI has been described since the late 1990s (e.g., Arrigo et al. 1997; Holm-Hansen and Hewes 2004; Hewes et al. 2008, 2009; Schloss et al. 2002, 2012, 2014; Schofield et al. 2017), but few data on NPP rates have been reported (e.g., Holm-Hansen and Mitchell 1991; Teira et al. 2012; García Muñoz et al. 2013, and references therein) describing maximum values of phytoplankton biomass associated with microplankton during December (~ 2.2 g m^{-2} day^{-1}), and high biomass of nanoplankton (90% of the total Chl-a) during February and March (Holm-Hansen and Mitchell 1991) after the seasonal retreat of ice. On the other hand, over the past three decades, many in situ measurements of NPP in the Drake Passage and Bransfield Strait show a wide range of spatial and seasonal variability, especially between shelf and open water stations (García Muñoz et al. 2013, 2014, and references therein). Although phytoplankton biomass is iron-limited in the ACC waters of the Drake Passage (e.g.,

Hopkinson et al. 2007, and references therein), high rates of NPP in the SSI archipelago are supported by bioavailable iron input into the Antarctic Peninsula-Bransfield Strait region (Ardelan et al. 2010). This may be the case in Deception Bay, where we found the highest total phytoplankton abundances for late summer 2013, which are possibly linked with natural iron fertilization occurring in a hydrothermal system (Fig. ESM_5, in online resource). At King George Island, phytoplankton maxima ($4–5.2 \times 10^6$ cells L^{-1}) dominated by nanoplankton and picoplankton were associated with small variations in low atmospheric pressure and low velocity winds (Kopczynska 2008). This dominance was also reflected in our late summer results where the nanoplankton size fraction represented > 50% of the total integrated Chl-*a* in the SSI.

Interestingly, bacterioplankton was the second contributor to the integrated carbon biomass in three of our sites (BC, BH, and RC) (Table 3). Bacterioplankton plays a fundamental role in the biogeochemical cycles of marine ecosystems (Cho and Azam 1990) because its use of dissolved organic matter mainly from the planktonic activity triggers the microbial trophic web (Azam 1998). Bacterioplankton was previously quantified at 0.27–5.31 µg C L^{-1} in the SSI (Llanos et al. 1991). Our results were slightly higher and in a similar range between 0.38 and 8.45 µg C L^{-1} (Table 2).

Our in situ NPP estimations provide a late summer view of the community functioning in SSI embayments. In general, during our 2013 and 2015 sampling periods, NPP changed temporally from heterotrophic to autotrophic trophic structure. NPP values were highly variable due to different CR rates that ranged from 0.07 to 5.67 g C m^{-2} day^{-1}. During 2015 in Collins Bay, GPP and CR were measured close to the front of Collins glacier and showed that the trophic mode can rapidly change from a heterotrophic to an autotrophic community after an 8-day period in a site proximal to a glacier (Table 4). Our results showed that high CR rates during late summer of 2015 were related to periods of higher abundances of heterotrophic dinoflagellates and bacterioplankton, as was shown at stations in Collins and Maxwell bays with the highest CR (5.7 and 2.0 g m^{-2} day^{-1}, respectively) (Table 4). In contrast, at the station distal from Collins glacier (Fildes Bay), NPP during late summer of 2013 and 2015 were positive because phytoplankton dominated in the surface water. Hanna, Maxwell, and Collins bays all showed single days with a negative balance on NPP due to their relatively higher proportions of microzooplankton and bacterioplankton (Table 4). Our results suggest that during late summer at these SSI sites, such local variability from autotrophy to heterotrophy could be influenced by reduced phytoplankton size to nanoplankton, accompanied by increased microzooplankton and bacterioplankton biomass, especially at glacier proximal sites.

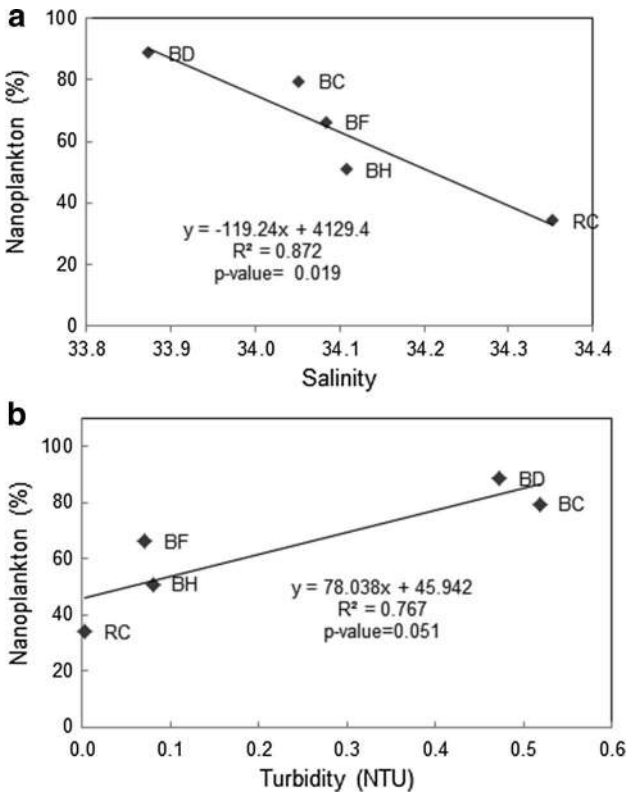

Fig. 7 Correlations between **a** nanoplankton Chl-*a* size fraction percentage (%) and salinity, and **b** nanoplankton Chl-*a* size fraction percentage (%) and turbidity at the four stations of this study. *BF* Fildes Bay, *BC* Chile Bay, *BH* Hanna Bay, *BD* Deception Bay, *RC* Rada Covadonga

Stations Rada Covadonga and Deception Bay were not influenced by the Bransfield Current. In fact, the water column at both locations showed different physical, chemical, and biological signatures. Station Rada Covadonga was affected by the activity of the PF and TWW, and Deception Bay by seasonal intrusion of UCDW (Fig. 1). All plankton groups were abundant and productivity proxies were the highest in Deception Bay (Fig. ESM_5, in online resource), possibly responding to a hydrothermal environment with high concentration of silicic acid (and possibly iron) and supported by an additional input of UCDW nutrients. Indeed, the high concentration of silicic acid at the station in Deception Bay is consistent with the low surface pH (6.9, Fig. 5c). Such UCDW nutrient input limits diatom populations on the middle and outer shelf because they depend on the renewal of the silica-rich UCDW (Prezelin et al. 2000). However, is not yet known if eddies located at the central Bransfield Strait enhance late summer productivity throughout nutrient transport via UCDW (Martinson and McKee 2012; Sangrà et al. 2017). These eddies have a maximum diameter of a few hundred meters and occur roughly four times per month, on average (Moffat et al. 2009). Local changes in ice cover in

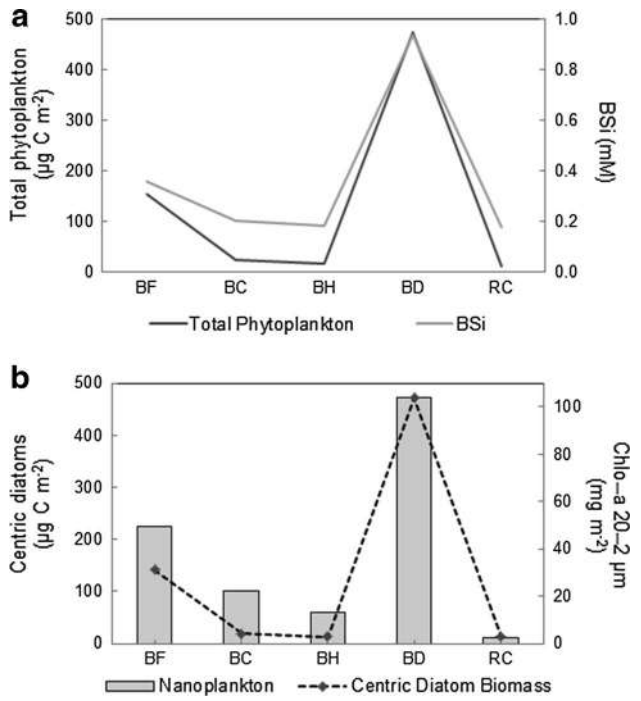

Fig. 8 **a** Integrated total phytoplankton biomass (mg C m^{-2}, *black line* vs. biogenic silica (*BSi*) concentration (mM, *gray line*). **b** Integrated centric diatom biomass (mg C m^{-2}, *black bar*) vs. integrated Chl-*a* of nanoplankton fraction (mg m^{-2}, *white square in dotted line*). Sites correspond to the five embayments of this study. *BF* Fildes Bay, *BC* Chile Bay, *BH* Hanna Bay, *BD* Deception Bay, *RC* Rada Covadonga

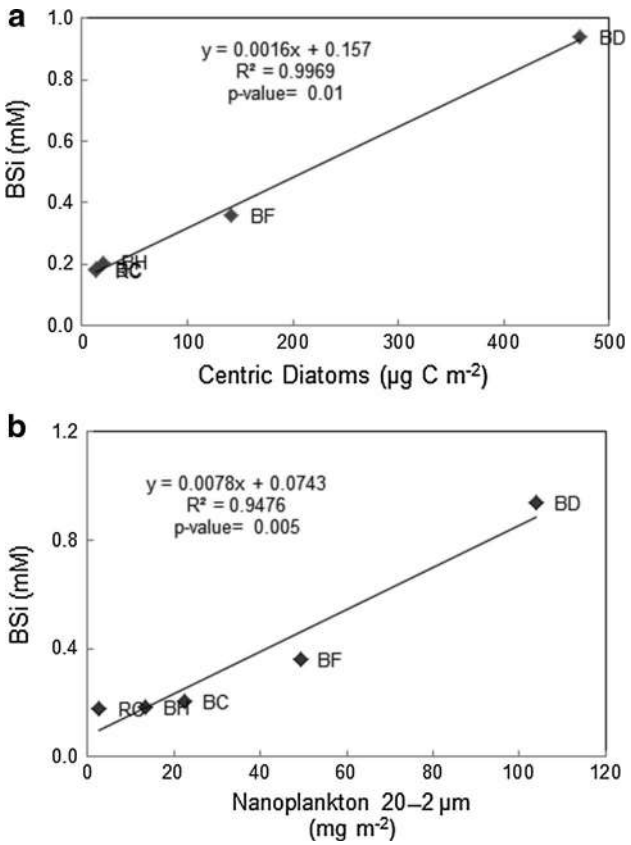

Fig. 9 Correlations between **a** BSi concentration (mM) and centric diatom integrated carbon biomass (mg C m^{-2}). **b** BSi concentration (mM) and integrated Chl-*a* nanoplankton size fraction (mg m^{-2}). at the surface layer (1–25 m depth) in the five embayments of this study. *BF* Fildes Bay, *BC* Chile Bay, *BH* Hanna Bay, *BD* Deception Bay, *RC* Rada Covadonga

this region could dilute the nutrient flux, especially during late summer. In this sense, we believe that long-term series on physical, chemical, and biological variability of the water column, as well as monitoring of local ice volume (including calving glaciers) and climatological variables, are crucial to provide accurate estimations, predictions, and reconstructions of summer phytoplankton productivity and size evolution in the SSI and in the WAP region. For example, Fildes Bay and Collins Bay are close to the scientific base "Profesor Julio Escudero" from INACH and, because they recently have achieved higher interest from the local marine sciences community, they should be nominated as reference points to continue long-term monitoring of phytoplankton dynamics considering pending regional and global changes.

Vertical salinity changes (1–50 m) were not detectable and CTD salinity values ~ 34 showed a homogeneous vertical structure of the water column at all sites except in Deception Bay, where a distinct surface layer of lower salinity (32.5) occurred at < 3 m depth (Fig. 5; Table ESM_1). Hanna Bay was characterized by high oxygen concentration ~ 8 ml L^{-1} at the surface, but with an abrupt decrease to ~ 6.7 ml L^{-1} above 4 m depth; however, the opposite pattern was observed in Deception Bay, with low oxygen concentration at the surface (~ 7.7 ml L^{-1}) and a fast recovery to ~ 8.2 ml L^{-1} at 2 m depth. The lower surface values may be related to higher SST due to the hydrothermal activity at the coast and a different biogeochemical context (see text 2 in online resource).

In the SSI region, the Chl-*a* maximum occurs at a salinity of ~ 34 where the upper mixed layer depth is shallow and surface waters are iron-replete (Hewes et al. 2009). When we integrated nanoplankton (20–2 µm), Chl-*a* correlated with averaged values (1–25 m) of salinity, and turbidity among stations, only salinity was significant ($R^2 = 0.87$; $p = 0.019$; and $R^2 = 0.77$; $p = 0.051$, respectively; Fig. 7a, b); turbidity values were very low and similar among stations (0–0.5 NTU). Nevertheless, in Deception Bay, the highest total phytoplankton biomass (474.2 mg C m^{-2}), the highest nanoplankton (88.6%), and diatom (95.1%) percentages were found at low surface salinity (Table 3). The coastal phytoplankton community composition at PALMER Station also showed that diatoms were present over the full range of in situ salinities (32–34.5) and over the full range of temperatures (−1.5 to 2.5 °C); however, nanoplankton was

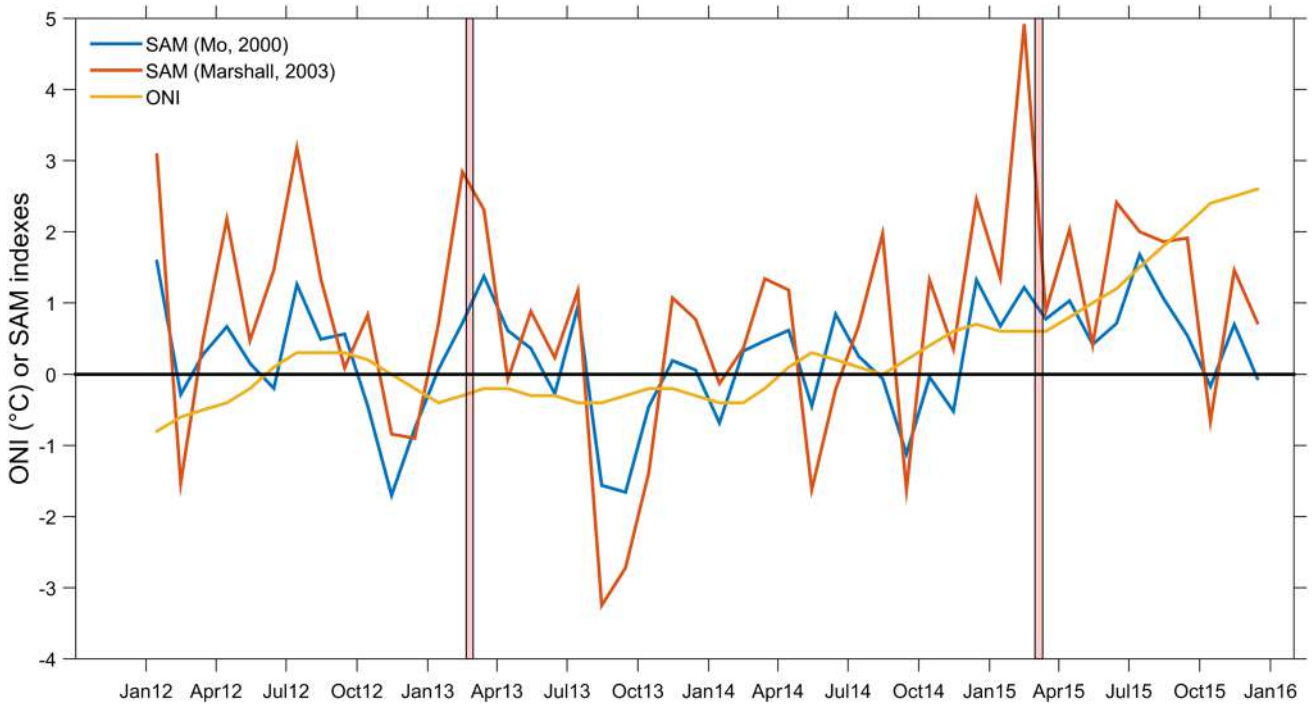

Fig. 10 Monthly time series of the Oceanic Niño Index (*ONI*) and Southern Anular Mode (*SAM*). ONI and SAM (Mo 2000) indexes were obtained from NOAA's Climate Prediction Center, and SAM (Marshall 2003) index from https://legacy.bas.ac.uk/met/gjma/sam.html. The shaded pink bars show the sampling periods. (Color figure online)

associated with lower salinities (32.5–33.75), colder water (−1 to 1 °C) (Schofield et al. 2017), and increased presence of sea-ice and glacial melt over time (Schofield et al. 2017).

February/March 2013 in situ measurements showed that integrated phytoplankton carbon biomass mirrored averaged BSi concentration at each station (Fig. 8a). with similar biomass distribution patterns of centric diatoms and integrated nanoplankton Chl-*a* (Fig. 8b). The proportions of diatoms of the total phytoplankton cells varied markedly over time, from 44% in 1996–1998 to 5% in 2003–2005 (Kopczynska 2008).

The BSi concentrations at our sampling sites were ten times higher (averages 0.18–0.94 mM) than values previously reported by Shiomoto and Ishii (1995) during summer along the coasts of the SSI (0.34–2.5 µM). Those authors also found high BSi concentrations near Deception Island. Finally, BSi was highly correlated with centric diatom biomass ($R^2 = 0.99$; $p = 0.01$; Fig. 9a) and integrated nanoplankton Chl-*a* ($R^2 = 0.94$; $p = 0.005$; Fig. 9b), which suggests that summer BSi concentration in the surface water column (1–25 m) is a suitable proxy for autotrophic diatom productivity in the SSI embayments.

Ducklow et al. (2007) previously reported the dominance of diatoms in the WAP, where blooms are supported by intrusions of nutrient-rich UCDW during spring and summer. In the Drake Passage, Bransfield Strait, and the WAP summer phytoplankton is dominated by microphytoplankton (> 20 µm) (Hewes et al. 2009). In these areas massive phytoplankton blooms only form in regions with proximity to meltwater and reduced exposure to storms, which are typical conditions of the coastal embayments of the Bransfield Strait region (Holm-Hansen and Mitchell 1991). In contrast, waters on the shelf and around the SSI have been characterized by high nanoplankton proportions (2–20 µm) (Kang and Lee 1995; Kawaguchi et al. 1999; Varela et al. 2002; Kopczynska 2008; García Muñoz et al. 2013), as we observed at our four SSI stations (BF, BH, BC, and BD). RC, which is influenced by the colder, saltier, and nutrient-poor TWW, is an exception to this nanoplankton dominance (Table 3). In late summer, increased nanoplankton abundances are related to selective grazing of microplankton cells by euphausiids and various species of copepods (Hewes et al. 2009; Schloss et al. 2014). During February 2013, exceptionally high wind speeds, the absence of a stratified surface layer, and early seasonal zooplankton grazing could explain high nanoplankton proportions in most of our study sites.

In this region, water mass exchange took place between coastal saline waters of the iron-replete WSSW arriving towards the NE flank of the SSI (Holm-Hansen et al.1997; Amos 2001; Holm-Hansen and Hewes 2004; Hewes et al. 2008) and the offshore fresher waters of the iron-poor Drake Passage. The El Niño-Southern Oscillation (ENSO) and

SAM fluctuations are the main influences on the oceanography of WAP ecosystems (Stammerjohn et al. 2012; Schloss et al. 2014; Schofield et al. 2017). The SAM is associated with the increased presence of the UCDW on the continental shelf (Schofield et al. 2017). During our sampling period, when ENSO (SAM) was normal (positive phase) (Fig. 10), SST and wind velocity increased in the AP (Lovenduski and Gruber 2005). In contrast, within the embayments, the SSTs were 0.1–0.3 °C colder than their long-term average, which could suggest intrusion of the UCDW waters into the embayments (especially in Deception Bay) or the windy conditions that prevented stratification during our fieldwork.

In the northern WAP, a decline in Chl-*a* is associated with an increase in cloudy days, a deepening of the upper mixed layer, stronger winds, and shorter sea-ice seasons along the marginal ice zone (Montes-Hugo et al. 2009). Our satellite data on wind and sea-ice cover, and the dominance of small nanoplankton Chl-*a*, agree with those observations. Moreover, cloudy days and intense wind mixing, especially in shallow embayments, causes light limitation for autotrophic organisms due to resuspension of sediment particles. We believe that, at our sampling sites in Collins Bay (proximal to the glacier front), a heterotrophic microbial food web was promoted during late summer with the dominance of bacterioplankton and microzooplankton (Table 4).

Deception Island differs from the other islands of the South Shetland archipelago by its active volcanic nature and the hydrothermal activity of the caldera. There is a constant flux of freshwater derived by snow melting at the beach all year, which lowers the surface water salinity. Despite this, Deception Bay had the highest abundances of plankton groups of all sites in our study. The expected iron contribution from volcanic activity, and seasonal instrusion of nutrient-rich UCDW could yield favorable conditions for plankton growth at Deception Bay. In fact, this site could constitute an opportunity to study natural phytoplankton fertilization in the SO.

Acknowledgements We acknowledge the financial support of this work to several projects and centers: FONDECYT–INACH 3130356, DID-UACh S-2015-28, Centers COPAS Sur-Austral CONICYT PIA PFB31 and FONDAP-IDEAL 15150003, and Nucleo Milenio Paleoclima del Hemisferio Sur NC120066. C. Aracena acknowledges the Institute of Marine and Limnological Sciences (ICML-UACh) and the Department of Oceanography of the University of Concepción for welcoming her to the laboratory facilities. C. Aracena also thanks Dr. Jose Luis Iriarte for providing technical personnel and equipment for fieldwork. Special thanks to Dr. Cristian Rodrigo, Dr. Javier Arata and to the Antarctic Chilean Institute (INACH) personnel for logistic and scientific support during fieldwork. We thank the captain and crew of the vessel AP 41 AQUILES for a very successful cruise. We sincerely thank Lilian Nuñez, Alejandro Avila, and Victor Acuña for laboratory work. Our special thanks to Dr. Irene Schloss for her valuable comments and suggestions to our work.

Compliance with ethical standards

Conflict of interest We do not have any conflicts of interest with the data presented in this scientific contribution.

References

Abram NJ, Mulvaney R, Wolff EW, Triest J, Kipfstuhl S, Trusel D, Vimeux F, Fleet L, Arrowsmith C (2013) Acceleration of snow melt in an Antarctic Peninsula ice core during the twentieth century. Nat Geosci 6:404–411

Amos AF (2001) A decade of oceanographic variability in summertime near Elephant Island, Antarctica. J Geophys Res 106:22401–22423

Ardelan MV, Holm-Hansen O, Hewes CD, Reiss CS, Silva NS, Dulaiova H, Steinnes E, Sakshaug E (2010) Natural iron enrichment around the Antarctic Peninsula in the Southern Ocean. Biogeosciences 7:11–25

Arrigo KR, Worthen D, Lizotte M, Dixon P, Dieckmann G (1997) Primary production in Antarctic Sea Ice. Science 276(5311):394–397

Arrigo KR, Worthen DL, Schnell A, Lizotte MP (1998) Primary production in Southern Ocean waters. J Geophys Res 103:15587–15600

Azam F (1998) Microbial control of oceanic carbon flux: the plot thickens. Science 280:694–696

Beers J, Stewart G (1970) Numerical abundance and estimated biomass of microzooplankton. Part VI. Bull Scripps Inst Oceanogr Univ Calif 17:67–87

Bentamy A, Fillon D (2012) Gridded surface wind fields from Metop/ASCAT measurements. Int J Remote Sens 33:1729–1754

Blindow N, Suckro SK, Ruckamp M, Braun M, Schindler M, Breuer B, Saurer H, Simoes JC, Lange MA (2010) Geometry and thermal regime of the King George Island ice cap, Antarctica, from GPR and GPS. Ann Glaciol 51:103–109

Blondeau-Patissier D, Gower JFR, Dekker AG, Phinn SR, Brandoc VE (2014) A review of ocean color remote sensing methods and statistical techniques for the detection, mapping and analysis of phytoplankton blooms in coastal and open oceans. Prog Oceanogr 123:123–144

Bodungen BV, Wunsch M, Fürderer H (1991) Sampling and analysis of suspended and sinking particles in the northern North Atlantic. In: Hurd DC, Spencer DW (eds) Marine particles: analysis and characterization. American Geophysical Union, Washington DC. https://doi.org/10.1029/GM063p0047

Boltovskoy D (1999) South Atlantic Zooplankton. Backhuys Publishers, Leiden, p 1706

Carrasco J (2007) Climatologia de la Peninsula Antartica y de la base Presidente Eduardo Frei Montalva. Direccion Meteorologica de Chile

Chin TM, Vazquez J, Armstrong E (2013) Algorithm theoretical basis document: a multi-scale, high-resolution analysis of global sea surface temperature. Jet Propulsion Laboratory, Pasadena

Cho BC, Azam F (1990) Biogeochemical significance of bacterial biomass in the ocean's euphotic zone. Mar Ecol Prog Ser 63:253–259

Cook AJ, Fox AJ, Vaughan DG, Ferrigno JG (2005) Retreating glacier fronts on the Antarctic Peninsula over the past half-century. Science 308:541–544

Cupp E (1943) Marine plankton diatoms of the west coast of North America, vol 5. University of California Press, Berkeley

Deppeler SL, Davidson AT (2017) Southern Ocean Phytoplankton in a changing climate. Front Mar Sci 4:40. https://doi.org/10.3389/fmars.2017.00040

Ducklow HW, Baker K, Martinson DG, Quetin LB, Ross RM, Smith RC, Stammerjohn SE, Vernet M, Fraser W (2007) Marine pelagic ecosystems: the West Antarctic Peninsula. Philos Tr Soc B 362:67–94

Edler L (1979) Recommendations for marine biological studies in the Baltic sea. Phytoplankton and Chlorophyll. Balt Mar Biol 5:1–38

Fuhrman JA, Azam F (1982) Thymidine incorporation as a measure of heterotrophic bacterioplankton production in marine surface waters: evaluation and field results. Mar Biol 66(2):109–120

García Muñoz C, Lubiàn L, García C, Marrero-Díaz A, Sangrà P, Vernet M (2013) A mesoscale study of phytoplankton assemblages around the South Shetland Islands (Antarctica). Polar Biol 36:1107–1123

Garibotti IA, Vernet M, Ferrario ME (2005) Annually recurrent phytoplanktonic assemblages during summer in the seasonal ice zone west of the Antarctic Peninsula (Southern Ocean). Deep-Sea Res Part I 52:1823–1841

Gonçalves-Araujo R, Silva de Souza M, Tavano VM, Eiras Garca CA (2015) Influence of oceanographic features on spatial and interannual variability of phytoplankton in the Bransfield Strait, Antarctica. J Mar Syst 142:1–15

Hass HC, Kuhn G, Monien P, Brumsack HJ, Forwick M (2010) Climate fluctuations during the past two millennia as recorded in sediments from Maxwell Bay, South Shetland Islands, West Antarctica. Geol Soc Lond Spec Publ 344: 243–260

Hernando M, Schloss IR, Malanga G, Almando O, Ferreyra GA, Aguiar MB, Puntarulo S (2015) Effects of salinity changes on coastal Antarctic phytoplankton physiology and assemblage composition. J Exp Mar Bio Ecol 466:110–119

Hewes CD, Reiss CS, Kahru M, Mitchell BG, Holm-Hansen O (2008) Control of phytoplankton biomass by dilution and mixing depth in the western Weddell-Scotia Confluence. Mar Ecol Prog Ser 366:15–29

Hewes CD, Reiss CS, Holm-Hansen O (2009) A quantitative analysis of sources for summertime phytoplankton variability over 18 years in the South Shetland Islands Antarctica. region. Deep-Sea Res Part I 56:1230–1241. https://doi.org/10.1016/j.dsr.2009.01.010

Holm-Hansen O, Hewes CD (2004) Deep chlorophyll-a maxima (DCMs) in Antarctic waters-I. Relationships between DCMs and the physical, chemical, and optical conditions in the upper water column. Polar Biol 27:699–710

Holm-Hansen O, Mitchell BG (1991) Spatial and temporal distribution of phytoplankton and primary production in the western Bransfield Strait region. Deep-Sea Res 38:961–980

Holm-Hansen O, Hewes CD, Villafañe VE, Helbling EW, Silva N, Amos AF (1997) Distribution of phytoplankton and nutrients in relation to different water masses in the area around Elephant Island, Antarctica. Polar Biol 18:145–153

Hopkinson BM, Mitchell BG, Reynolds RA, Wang H, Selph KE, Measures CL, Hewes CD, Holm-Hansen O, Barbeau KA (2007) Iron limitation across chlorophyll gradients in the southern Drake Passage: phytoplankton responses to iron addition and photosynthetic indicators of iron stress. Limnol Oceanogr 52:2540–2554

Kang SH, Lee SH (1995) Antarctic phytoplankton assemblage in the western Bransfield Strait region, February 1993: composition, biomass and mesoscale distributions. Mar Ecol Prog Ser 129:253–267

Kang JS, Kang SH, Lee JH, Lee SH (2002) Seasonal variation of microalgal assemblages at a fixed station in King George Island, Antarctica, 1996. Mar Ecol Prog Ser 229:19–32

Kawaguchi S, Ichii T, Naganobu M (1999) Green krill, the indicator of micro- and nano-size phytoplankton availability to krill. Polar Biol 22:133–136

Khim BK, Shim J, Yoon HI, Kang YC, Jang YH (2007) Lithogenic and biogenic particle deposition in an Antarctic coastal environment (Marian Cove, King George Island): seasonal patterns from a sediment trap study. Estuar Coast Shelf Sci 73:111–122

Klinck J (1998) Heat and salt changes on the continental shelf west of the Antarctic Peninsula between January 1993 and January 1994. J Geophys Res 103:7617–7636

Kopczynska E (2008) Phytoplankton variability in Admiralty Bay, King George Island, South Shetland Islands: six years of monitoring. Pol Polar Res 29(2):117–139

Llanos A, Acevedo A, Troncoso A, González H, Sandra M, Iriarte J, Bernal P (1991) Abundancia y producción secundaria bacteriana en el área de las islas Shetland del Sur, Antártica. Ser Cien INACH 41:55–63

Lovenduski N, Gruber N (2005) Impact of the Southern Annular Mode on Southern Ocean circulation and biology. Geophys Res Lett 32:11

Marshall GJ (2003) Trends in the Southern Annular Mode from observations and reanalyses. J Clim 16:4134–4143

Martinson DG, McKee DC (2012) Transport of warm Upper Circumpolar Deep Water onto the western Antarctic Peninsula continental shelf. Ocean Sci 8:433–442

Martinson DG, Stammerjohn S, Iannuzzi R, Smith RC, Vernet M (2008) Western Antarctic Peninsula physical oceanography and spatio–temporal variability. Deep Sea Res Part II 55:1964–1987

Meredith MP, King JC (2005) Rapid climate change in the ocean to the west of the Antarctic Peninsula during the second half of the twentieth century. Geophys Res Lett 32:L19604. https://doi.org/10.1029/2005GL024042

Moffat C, Owens B, Beardsley RC (2009) On the characteristics of Circumpolar Deep Water intrusions to the west Antarctic Peninsula Continental Shelf. J Geophys Res 114:C5

Moline MA, Claustre H, Frazer TK, Schofield O, Vernet M (2004) Alteration of the food web along the Antarctic Peninsula in response to a regional warming trend. Glob Change Biol 10:1973–1980

Monien P, Schnetger B, Brumsack HJ (2011) A geochemical record of late Holocene palaeoenvironmental changes at King George Island (maritime Antarctica). Antarct Sci 23:255–267

Montes-Hugo M, Vernet M, Martinson D, Smith R, Iannuzzi R (2008) Variability on phytoplankton size structure in the western Antarctic Peninsula (1997–2006). Deep-Sea Res Part II 55:2106–2117

Montes-Hugo MA, Doney SC, Ducklow HW, Fraser W, Martinson D, Stammerjohn SE, Schofield O (2009) Recent changes in phytoplankton communities associated with rapid regional climate change along the Western Antarctic Peninsula. Science 323:1470–1473

Mura MP, Satta MP, Agustí S (1995) Water-mass influences on Summer Antarctic phytoplankton biomass and community structure. Polar Biol 15:15–20

Niiler PP, Amos AF, Hu JH (1991) Water masses and 200 m relative geostrophic circulation in the western Bransfield Strait region. Deep-Sea Res Part II 38:943–959

Orsi AH, Whitworth TW III, Nowlin WD Jr (1995) On the meridional extent and fronts of the Antarctic Circumpolar Current. Deep Sea Res Part I 42:641–673

Parsons TR, Maita Y, Lali CM (1984) A manual of chemical and biological methods for seawater analysis. Pergamon, Oxford, p 173

Porter KG, Feig YS (1980) The use of DAPI for identifying and counting aquatic microflora. Limnol Oceanogr 25(5):943–948

Powell R, Domack E (2002) Modern glaciomarine environments. In: Menzies J (ed) Modern and past glacial environments. Butterworth–Heinemann, Boston

Prezelin B, Hofmann E, Manegelt C, Klinck JM (2000) The linkage between Upper Circumpolar Deep Water (UCDW) and phytoplankton assemblages on the west Antarctic Peninsula continental shelf. J Mar Res 58:165–202

Ragueneau O, Savoye N, Del Amo Y, Cotten J, Tardiveau B, Leynaert A (2005) A new method for the measurement of biogenic silica in suspended matter of coastal waters: using Si: Al ratios to correct for the mineral interference. Cont Shelf Res 25:697–710

Reynolds CS (1997) Vegetation processes in the pelagic: a model for ecosystem theory. Ecology Institute, Oldendorf

Rhein M, Rintoul SR, Aoki S, Campos E, Chambers D, Feely RA, Gulev S, Johnson GC, Josey SA, Kostianoy A, Mauritzen C, Roemmich D, Talley LD, Wang F (2013) Observations Ocean. In: Stocker TF, Qin D, Plattner GK, Tignor M, Allen SK, Boschung J, Nauels A, Xia Y, Bex V, Midgley PM (eds) Climate Change 2013: the physical science basis. Contribution of Working Group I to the Fifth Assessment Report of the Intergovernmental Panel on Climate Change. Cambridge University Press, Cambridge, New York

Rückamp M, Blindow N (2012) King George Island ice cap geometry updated with airborne GPR measurements. Earth Syst Sci Data 4:23–30

Rückamp M, Braun M, Suckro S, Blindow N (2011) Observed glacial changes on the King George Island ice cap, Antarctica, in the last decade. Glob Planet Change 79:99–109

Saba GK, Fraser WR, Saba V, Iannuzzi R, Coleman KE, Doney SC, Ducklow HW, Martinson DG, Miles TN, Patterson-Fraser DL, Stammerjohn SE, Steinberg DK, Schofield O (2014) Winter and spring controls on the summer food web of the coastal West Antarctic Peninsula. Nat Commun 5:4318. https://doi.org/10.1038/ncomms5318

Sangrà P, García-Muñoz C, García CM (2014) Coupling between the upper ocean layer variability and size-fractionated phytoplankton in a no nutrient environment. Mar Ecol Prog Ser 499:35–46

Sangrà P, Stegner A, Hernández-Arencibia M, Marrero-Díaz A, Salinas C, Aguiar-González B, Henríquez-Pastene C (2017) The Bransfield gravity current. Deep-Sea Res Part I 119:1–15

Savtchenko A, Ouzounov D, Ahmad S, Acker J, Leptoukh G, Koziana J, Nickless D (2004) Terra and Aqua MODIS products available from NASA GES DAAC. Adv Space Res 34:710–714

Schloss IR, Ferreyra GA (2002) Primary production, light and vertical mixing in Potter Cove, a shallow Bay in the maritime Antarctic. Polar Biol 25:41–48

Schloss IR, Ferreyra G, Ruiz-Pino D (2002) Phytoplankton biomass in Antarctic shelf zones: a conceptual model based on Potter Cove, King George Island. J Mar Syst 36:129–143

Schloss IR, Doris A, Moreau S, Demers S, Bers V, González O, Ferreyra G (2012) Response of phytoplankton dynamics to 19-year (1991–2009) climate trends in Potter Cove (Antarctica). J Mar Syst 92:53–66

Schloss IR, Wasilowska A, Dumont D, Almandoz GO, Hernando MP, Michaud- Temblay CA, Saravia L, Rzepecki M, Monien P, Kopczynska EE, Bers AV, Ferreyra GA (2014) On the phytoplankton bloom in coastal waters of southern King George Island (Antarctica) in January 2010: an exceptional feature? Limnol Oceanogr 59:195–210

Schofield O, Ducklow HW, Martinson DG, Meredith MP, Moline MA, Fraser WR (2010) How do polar marine ecosystems respond to rapid climate change? Science 328:1520–1523

Schofield O, Saba G, Coleman K, Carvalho F, Couto N, Ducklow H, Fink Z, Irwin A, Khal A, Milesa T, Montes-Hugo M, Stammerjohn S, Waite N (2017) Decadal variability in coastal phytoplankton community composition in a changing West Antarctic Peninsula. Deep Sea Res I 124:42–54

Sherr EB, Sherr BF (1994) Bacterivory and herbivory: key roles of phagotrophic protists in pelagic food webs. Microb Ecol 28(2):223–235

Shiomoto A, Ishii H (1995) Distribution of biogenic silica and particulate organic matter in coastal and oceanic surface waters off the South Shetland Islands in summer. Polar Biol 15:105–113

Simms AR, Milliken KT, Anderson JB, Wellner JS (2011) The marine record of deglaciation of the South Shetland Islands, Antarctica since the Last Glacial Maximum. Quat Sci Rev 30:1583–1601

Simoes JC, Gobmann H, Delmas RJ, Moskalevsky MY (2004) Glaciological research in King George Island: missions and developments in the 1990s. Pesquisa Antarct Brasileira 4:1–8

Smith RC, Dierssen HM, Vernet M (1996) Phytoplankton biomass and productivity in the Western Antarctic Peninsula region. Foundations for ecological research West of the Antarctic Peninsula. Antarct Res S 70:333–356

Spreen G, Kaleschke L, Heygster G (2008) Sea ice remote sensing using AMSR-E 89 GHz channels. J Geophys Res 113:C02S03. https://doi.org/10.1029/2005JC003384

Stammerjohn SE, Martinson DG, Smith RC, Yuan X, Rind D (2008) Trends in Antarctic annual sea ice retreat and advance and their relation to ENSO and Southern annular mode variability. J Geophys Res 113:C03S90. https://doi.org/10.1029/2007JC004269

Stammerjohn S, Massom R, Rind D, Martinson D (2012) Regions of rapid sea ice change: an inter-hemispheric seasonal comparison. Geophys Res Lett. https://doi.org/10.1029/2012GL050874

Strickland JDH, Parsons TR (1972) A practical handbook of seawater analysis, Fisheries Research Board of Canada

Teira E, Mouriño-Carballido B, Martínez-García S, Sobrino C, Ameneiro J, Hernández-León S, Vázquez E (2012) Controls of primary production and bacterial carbon metabolism around South Shetland Islands. Deep-Sea Res Part I 69:70–81

Thomas ER, Marshall G, McConnell JR (2008) A doubling in snow accumulation in the western Antarctic Peninsula since 1850. Geophys Res Lett 35:L01706. https://doi.org/10.1029/2007GL032529

Thompson DWJ, Solomon S (2002) Interpretation of recent Southern Hemisphere climate change. Science 296:895–899

Tomas C (1997) Identifying marine phytoplankton. Academic, St. Petersburg

Utermöhl H (1958) Zur Vervollkommnung der quantitativen Phytoplankton-Methodik. Mitt. Verh Int Verein Theoret Angew Limnol 9:1–39

Varela M, Fernandez E, Serret P (2002) Size-fractionated phytoplankton biomass and primary production in the Gerlache and south Bransfield Straits (Antarctic Peninsula) in Austral summer 1995–1996. Deep-Sea Res Part II 49:749–768

Vaughan DG, Comiso JC, Allison I, Carrasco J, Kaser G, Kwok R, Mote P, Murray T, Paul F, Ren J, Rignot E, Solomina O, Steffen K, Zhang T (2013) Observations cryosphere. In: Stocker TF, Qin D, Plattner G-K, Tignor M, Allen SK, Boschung J, Nauels A, Xia Y, Bex V, Midgley PM (eds) Climate change 2013 the physical science basis. Contribution of Working Group I to the Fifth Assessment Report of the Intergovernmental Panel on Climate Change. Cambridge University Press, Cambridge

Villafañe V, Helbling E, Holm-Hansen O (1995) Spatial and temporal variability of phytoplankton biomass and taxonomic composition around Elephant Island, Antarctica, during the summers of 1990–1993. Mar Biol 123:677–686

Winkler LW (1888) Die Bestimmung des in Wasser gelösten Sauerstoffen. Ber Dtsch Chem Ges 21:2843–2855